



ELM-based adaptive neuro swarm intelligence techniques for predicting the California bearing ratio of soils in soaked conditions



Abidhan Bardhan ^{a,*}, Pijush Samui ^a, Kuntal Ghosh ^b, Amir H. Gandomi ^c,
Siddhartha Bhattacharyya ^d

^a Civil Engineering Department, National Institute of Technology (NIT) Patna, India

^b Computer and Communication Sciences Division, Indian Statistical Institute, Kolkata, India

^c Faculty of Engineering and Information Technology, University of Technology Sydney, Ultimo, NSW 2007, Australia

^d Rajnagar Mahavidyalaya, Birbhum, West Bengal, India

ARTICLE INFO

Article history:

Received 10 December 2020

Received in revised form 4 June 2021

Accepted 5 June 2021

Available online 8 June 2021

Keywords:

Swarm intelligence

Soft computing

CBR

DFC

Indian Railways

Particle swarm optimization

ABSTRACT

This study proposes novel integration of extreme learning machine (ELM) and adaptive neuro swarm intelligence (ANSI) techniques for the determination of California bearing ratio (CBR) of soils for the subgrade layers of railway tracks, a critical real-time problem of geotechnical engineering. Particle swarm optimization (PSO) with adaptive and time-varying acceleration coefficients (TAC) was employed to optimize the learning parameters of ELM. Three novel ELM-based ANSI models, namely ELM coupled-modified PSO (ELM-MPSO), ELM coupled-TAC PSO (ELM-TPSO), and ELM coupled-improved PSO (ELM-IPSO) were developed for predicting the CBR of soils in soaked conditions. Compared to standard PSO (SPSO), the modified and improved version of PSO are capable of converging to a high-quality solution at early iterations. A detailed comparison was made between the proposed models and other conventional soft computing techniques, such as conventional ELM, artificial neural network, genetic programming, support vector machine, group method of data handling, and three ELM-based swarm intelligence optimized models (ELM-based grey wolf optimization, ELM-based slime mould algorithm, and ELM-based Harris hawks optimization). Experimental results reveal that the proposed ELM-based ANSI models can attain the most accurate prediction and confirm the dominance of MPSO over SPSO. Considering the consequences and robustness of the proposed models, it can be concluded that the newly constructed ELM-based ANSI models, especially ELM-MPSO, can solve the difficulties in tuning the acceleration coefficients of SPSO by the trial-and-error method for predicting the CBR of soils and be further applied to other real-time problems of geotechnical engineering.

© 2021 Elsevier B.V. All rights reserved.

1. Introduction

Railways provide one means of transportation for transferring goods and passengers by which wheeled vehicles run on rails installed on tracks. Tracks usually consist of steel rails fitted to sleeper cars that are installed over ballast cushions. The entire track systems are laid on a prepared foundation over the natural ground surface called a Permanent way (P-way). Special guidelines are followed during the construction of P-ways so that the train's load can be uniformly distributed and transferred to the sub-soil. In general, railways, roadways, and airport runways require the construction of a proper sub-base layer, which is often the main load bearing layer, while the upper layer of the

sub-soil is prepared as a sub-base or subgrade. The sub-base or prepared subgrade layers should satisfy several engineering and technical requirements, such as settlement criteria, subgrade reaction, bearing capacity, swelling properties, etc. Thus, a method for assessing such layers is of utmost necessity in geotechnical engineering, especially for railways, roadways, and runways. The California bearing ratio (CBR) is often used to measure the shear strength and stiffness modulus of a subgrade, which is an indirect measure that compares the strength of the subgrade material to strength of the standard crushed rock sample [1]. CBR is the ratio of force per unit area required to penetrate a soil mass to that required for the standard material. To obtain this ratio, a standard circular piston with 1.27 mm/min velocity is used to penetrate the soil sample during experimentation either in a laboratory or in the field [2]. Generally, the laboratory test is performed on compacted soil samples with the optimum moisture content (OMC), while field CBR tests are conducted at the natural ground surface level, prepared subgrade level, or on a level surface of the test pit at construction sites.

* Corresponding author.

E-mail addresses: abidhan@nitp.ac.in (A. Bardhan), pijush@nitp.ac.in (P. Samui), kuntalghos@gmail.com (K. Ghosh), gandomi@uts.edu.au (A.H. Gandomi), dr.siddhartha.bhattacharyya@gmail.com (S. Bhattacharyya).

Nomenclature		Important symbols	
P-way	Permanent way	c_1	Cognitive coefficient
CBR	California bearing ratio	c_2	Social coefficient
OMC	Optimum moisture content	w	Inertia weight
PI	Plasticity index	w_{max}	Maximum inertia weight
LI	Liquidity indices	w_{min}	Minimum inertia weight
LL	liquid limit	v	Particle velocity
AL	Atterberg's limits	t	Current iteration number
NCHRP	National Cooperative Highway Research Program	k	Maximum number of iterations
ANN	Artificial neural network	r_1, r_2	Random parameters
GP	Genetic Programming	c_{1max}	Maximum value of c_1
SVM	Support vector machine	c_{1min}	Minimum value of c_1
GEP	Gene expression programming	c_{2max}	Maximum value of c_2
GMDH	Group method of data handling	c_{2min}	Minimum value of c_2
ANFIS	Adaptive neuro-fuzzy inference system	c_{max}	Maximum value of c
GRNN	General regression neural network	c_{min}	Minimum value of c
ELM	Extreme learning machine	N_h	Number of hidden neurons
ML	Machine learning	k	k -fold cross-validation
CSC	Conventional soft computing	y_i	Experimental i^{th} value
R^2	Determination coefficient	y_{avg}	Mean of actual values
OAs	Optimization algorithms	\tilde{y}_i	Predicted i^{th} value
PSO	Particle swarm optimization	A_{I10}	Accuracy index
MPSO	Modified PSO	n_s	Swarm size
TPSO	PSO with time-varying acceleration coefficients	ε_i	absolute error
IPSO	Improved PSO	H_0	Null hypothesis
SPSO	Standard PSO	H_A	Alternate hypothesis
GWO	Grey wolf optimization	α	level of significance
SMA	Slime mould algorithm	C1	Case 1
HHO	Harris hawks optimization	C2	Case 2
ANSI	Adaptive neuro swarm intelligence	C3	Case 3
DFC	Dedicated Freight Corridor	C4	Case 4
GQFC	Golden Quadrilateral Freight Corridor		
WDFC	Western Dedicated Freight Corridor		
EDFC	Eastern Dedicated Freight Corridor		
G	Gravel content		
S	Content of sand		
S&C	Silt and clay content		
MDD	Maximum dry density		
CL	Clay with low plasticity		
CI	Clay with intermediate plasticity		
SC	Clayey sand		
ML	Low plasticity silt		
SM	Silty sand		
TR	Training		
TS	Testing		
VAF	Variance account for		
PI	Performance index		
WI	Willmott's index of agreement		
MAE	Mean absolute error		
MAPE	Mean absolute percentage error		
MBE	Mean bias error		
RMSE	Root mean square error		
A_{I10}	Accuracy index		

While laboratory tests are performed on compacted soil samples with OMC in un-soaked and soaked conditions, as mentioned above, they can also be carried out on natural soils. The

obtained results are then compared with the standard value to estimate the strength of the soil sample, which are quite significant for geotechnical engineering and its related structures, such as railway embankments, airport runways, abutments and piers of bridges, highway embankments, etc. Thus, it is necessary to consider additional measures when performing such laboratory tests. Engineers, practitioners, and industry personnel always encounter difficulties in obtaining actual CBR values for design purposes, often obtaining inadequate soil investigation results. Moreover, the CBR test is laborious and time-consuming, and the results obtained in laboratory sometimes are inaccurate due to the disturbance of samples, negligence during testing, and poor testing facilities [2,3]. Hence, researchers have developed approximation models for predicting CBR values by considering the index properties of soils as the only governing parameters. Several studies have demonstrated the effect of soil types and

their basic properties on CBR, subsequently identifying several correlations between CBR and other soil parameters [1,4–9].

For instance, Black [4] developed a model for the estimation of CBR of cohesive soils and discovered that the correlation between CBR and plasticity index (PI) for different liquidity indices (LI) holds valid only for saturated soils. Johnson and Bhatia [5] presented the concept of the suitability index to determine the CBR value, while Agarwal and Ghanekar [6] developed a correlation equation between the Atterberg's limits (AL) and CBR, but the developed equation is not able to find any significant correlation [3]. The authors also developed improved correlation between OMC, liquid limit (LL), and CBR, however, the author of [3] mentioned that the correlation was only of sufficient accuracy. Stephens [1] used archival data from the Natal Roads Department of Pietermaritzburg to assess the performance of the existing models and defined the correlation between CBR and various soil parameters, subsequently discovering these models to be generally unsatisfactory. The latter study further investigated the lack of an appropriate correlation for universal use and thus, presented a new relationship between maximum swell and CBR, and the impact of clay fraction on the CBR. To obtain the minimum CBR for shrinking and non-shrinking soils, the use of the gradation and shrinkage was proposed. Al-Refeai and Al-Suhaimi [7] performed a comprehensive study on the prediction of CBR using dynamic cone penetrometer test data. In the latter study, a graphical representation showed the relationship between moisture content, dry density with CBR, and penetration depth for different types of soils. The relationship between penetration depth and CBR was furnished for the tested soils under different moisture content and density conditions. Results obtained in each case were found satisfactory. In the U.S., the National Cooperative Highway Research Program (NCHRP) [8] suggested two best-fitted equations that express the relationship between the CBR and index properties of soil for clean and coarse grain soils (non-plastic soil). Kin [9] calculated the CBR values as per BS 1377-4:1990 by correlating the grain sizes and measured CBR values for coarse-grained and fine-grained soils. Kin further showed that the correlation equations of CBR given by NCHRP are unable to predict the measured CBR values correctly for coarse-grained soils, which in turn indicates the limitations of NCHRP's equation, i.e., the developed equation is applicable for clean coarse-grained soil only. In contrast, for fine-grained soils, an unhealthy/inaccurate correlation between the actual and estimated values of CBR from the NCHRP's equation was obtained. In addition, several studies were performed to predict the CBR of soils by using simple and multiple regression techniques [2,10–17]. However, a detailed review of these studies reveals that acceptable correlations could not be attained in many cases [3]. Most of the proposed empirical equations neither have a high degree of accuracy nor any generalized solutions, which is mainly due to the inadequate representation of soil properties, presence of intricate relationships among the parameters, and inconsequential methods of calculations [2,3].

On the contrary, progress in the field of soft computing encompasses several topics, including geotechnical engineering applications. New models and procedures, especially those based on soft computing techniques, enable researchers to gain insight into the most intricate systems in different ways. Application of soft computing techniques, such as the artificial neural network (ANN), support vector machine (SVM), gene expression programming (GEP), group method of data handling (GMDH), adaptive neuro-fuzzy inference system (ANFIS), general regression neural network (GRNN), and extreme learning machine (ELM), is gaining increasing popularity in the field of geotechnical engineering [2,3,11,12,14,18–28].

In geotechnical engineering, the estimation of CBR of soils is an important criterion for measuring the stiffness modulus

of subgrade layers. In the last decade, several machine learning (ML) models, such as ANN [2,3,12,14,18,20–22,25–27,29], GEP [3,23], SVM [23,30], and GMDH [24], have been used to construct predictive models for CBR based on basic soil properties, such as AL, compaction characteristics, and particle size of soil. It is pertinent to note that most of these models were developed based on conventional soft computing (CSC) models, like ANN and SVM, and higher predictive accuracy (ranging from 0.90 to 1.00 based on determination coefficient (R^2) value) was attained in many cases [2,11,15,19,21,22,26,27]. However, these studies cannot be considered very reliable [31], due to the fact that the models were developed and validated with small datasets (total number of observations were between 20 and 124 only). In addition, the predictive accuracy using CSC models appeared to decrease for larger datasets (total number of samples were in the range of 358 to 389). The prediction performance was in the range of 0.78 to 0.80 based on R^2 value [23,25]. This reduction in accuracy may be due to the following reasons: the absence of a wide range of input combinations; complex data type; and improper training of ML algorithms. In addition, overfitting is a major concern to the success rate of CSC techniques, may also be one of the reasons. Moreover, these CSC models, such as ANN, produce undesirable results due to their weakness in finding the exact global optimum [32,33]; thus, several works have been conducted to enhance their performance [32,34–46]. In addition, ANN is more likely to get stuck in local minima, leading to erroneous results [32,41]. To overcome these issues, researchers have developed several hybrid models by integrating optimization algorithms (OAs) and CSC models to search for the exact global minimum instead of finding the local minima [39,41]. Hybridization of OAs and CSC techniques balance the exploration and exploitation processes and generate optimized values of learning parameters (weights and biases), which in turn are used to enhance the performance of the CSC techniques [34].

Thus, a widely-used population-based meta-heuristic OA, i.e., particle swarm optimization (PSO), is employed in the present study to improve the performance of an efficient ML model, ELM. Note that, although ELM is a simple ML algorithm that shadows the ANN's structure, its working principle is slightly different than that of ANN. Specifically, ELM uses a proper analytical formulation to predict the desired output and provides good generalization performance at extremely fast learning speeds [47]. Instead of having four learning parameters like ANN, ELM has only two learning parameters: hidden weights and hidden biases. Typically, these learning parameters play an essential role in determining output weights; hence, the random selection of these parameters may affect the performance in both the training and testing stages. Therefore, optimized values of weights and biases can be used to theoretically solve this problem. For this purpose, PSO was employed to optimize the learning parameters of ELM, thus producing the hybrid ELM-PSO model.

As stated earlier, PSO is a population-based meta-heuristic OA that has gained immense popularity and use over the last decade due to its ease of implementation and quick converging ability to a reasonably good solution [48]. This allows PSO to be used on functions where the gradient is either unavailable or computationally expensive to obtain. However, the stochastic nature [48,49] of PSO often inhibits it from observing the characteristics predicted by the theoretical model directly. Therefore, it may require an infinite number of iterations to guarantee that the global minimum will be reached [50]. As indicated by Bui et al. [37], the searching space of the PSO parameters limits the position of the particles, making it difficult to locate the exact global minimum, and thus requires a large number of iterations to converge. This indicates that the probability of locating the exact global minimum in a finite number of iterations is relatively small [50]. Also, the authors of [50,51] state that locating

global minimum is always challenging for all minimization problems; and hence, the main focus should be on the convergence behaviour for finding the exact global minimum [50].

The main parameters of PSO include the acceleration coefficients (c_1 and c_2) and inertia weight (w), where c_1 (cognitive coefficients) and c_2 (social coefficients) have a significant effect on the performance of PSO [48]. Note that these parameters are deterministic in nature and should be tuned properly to control the convergence towards the global best solution. In general, the values of c_1 and c_2 are selected between 1 and 2 to perform the exploration and exploitation process [34,39,41,42]. Since there is no specific rule or criteria for choosing the optimum values of acceleration coefficients, researchers use the trial-and-error approach [36,37,39,43,44,52], to find the most suitable searching space for the problem at hand, which is not only a time-consuming task but also generates multiple inappropriate solutions.

Considering these issues, this study was motivated to implement adaptive and time-varying acceleration coefficients instead of using their fixed values with the trial-and-error approach. Herein, three different strategies, namely modified PSO (MPSO) proposed by [50], PSO with time-varying acceleration coefficients (TPSO) proposed by [53], and improved PSO (IPSO) proposed by [48], were used to tune the acceleration coefficients (c_1 and c_2) of three ELM-based models. Then, these models, namely ELM-based MPSO (ELM-MPSO), ELM-based TPSO (ELM-TPSO), and ELM-based IPSO (ELM-IPSO), were employed to predict the CBR of soils in soaked conditions. Compared to standard PSO (SPSO), the modified and improved version of PSO can evade local minima trapping issues, which in turn enhances the search capability and convergence rate [48,50,53]. For a more detailed comparison, the performance of PSO with fixed acceleration coefficients was examined through the ELM-PSO, ELM-GWO (ELM-based grey wolf optimization), ELM-SMA (ELM-based slime mould algorithm), and ELM-HHO (ELM-based Harris hawks optimization) models. Further, the generalization capabilities of the proposed ELM-based adaptive neuro swarm intelligence (ANSI) models (ELM-MPSO, ELM-TPSO, and ELM-IPSO) were compared with other CSC models, including classical ELM and ANN, GP, SVM, and GMDH. For this purpose, a wide range of CBR test data of soil was collected from an ongoing railway project in India and used to develop the predictive models. It is pertinent to mention that, for the first time, this study presents the application of adaptive and time-varying acceleration coefficients to control the exploration and exploitation process of PSO for predicting the CBR of soaked soils, one of the most critical real-time problems of civil engineering, using ELM-based ANSI models.

The remainder of this study is organized as follows. Section 2 presents the methodological approach, followed by details of the study area in Section 3. Section 4 discusses the descriptive statistics and statistical analysis. The realizations of the developed models are described in the results and discussion in Section 5, and finally, a summary and the conclusions are presented in Section 6.

2. Methodology

This section describes the development of soft computing techniques by first presenting the methodology of ELM, followed by the theoretical background of PSO, MSPO, TPSO, and IPSO. A brief overview of CSC models (ANN, GP, SVM, and GMDH) and other OAs (GWO, SMA, and HHO) used in this study are also presented. Finally, the hybridization approach for developing the ELM-based meta-heuristic models is introduced.

2.1. Extreme Learning Machine (ELM)

ELM, proposed by [47], is a simple, fast, and efficient ML algorithm with a single layer of hidden neurons, called the single layer feedforward neural network, and is used for classification, clustering, regression, and function approximation. The structure of this ML algorithm consists of an input layer, one hidden layer, and an output layer, with one or more numbers of neurons in each layer. The weights between the input and hidden nodes and biases of hidden neurons are randomly assigned during the course of training, which remains constant throughout the analytical operation. In contrast, the weights between the hidden nodes and output(s) can be trained very fast. ELM exhibits a more generalized performance with low computational cost compared to other back-propagation ML algorithms. The structure of the ELM network with the input, hidden, and output layers is shown in Fig. 1.

The output of a model with p input features and n samples of the dataset $X = \{x_t \in R^p\}, t_p = \{1, 2, \dots, n\}$ can be written as:

$$o_i(t) = m_i^T h(t_p) \quad (1)$$

where $m_i \in R^q, i \in \{1, 2, \dots, o\}$ represents the weight vector, which connects the hidden neurons to the i th output neuron; $h(t_p) \in R^q$ denotes the output vector of hidden neurons for an input pattern of $x_t \in R^p$; and the output vector $h(t_p)$ can be expressed as:

$$h(t_p) = [f(w_1^T x(t_p) + b_1), f(w_2^T x(t_p) + b_2), \dots, f(w_q^T x(t_p) + b_q)] \quad (2)$$

where (b_1, b_2, \dots, b_q) represents the bias of hidden neurons; $w_k \in R^p$ denotes the weight vector of k th hidden neurons; and the function $f(\cdot)$ is the activation function. It should be noted that the bias (b_k) and weight vector (w_k) are generated from a Gaussian distribution in a random manner. Using the bias and weight vector, the matrix of the hidden layer output H ($q \times n$ matrix) can be formed; and the $q \times l$ matrix called the weight matrix (M) can be calculated using 'Moore-Penrosepseudo inverse' method [54–56] in the form of:

$$M = (H \times H^T)^{-1} H \times D^T \quad (3)$$

where $D = [d(1), d(2), \dots, d(n)]$ denotes a $l \times n$ matrix; and the t_p^{th} column is the real largest vector $d(t_p) \in R^l$. With all the specified parameters of the network, the class label for the 'new input' feature can be determined using $Y = \arg \max \{o_i\}, i = \{1, 2, \dots, l\}$, where Y is the predicted class label. Several applications of this ML technique are available in the literature, and researchers use this technique to predict the desired output in all branches of engineering [39,57,58].

2.2. Particle Swarm Optimization (PSO)

PSO, introduced by Kennedy and Eberhart [59], is a population-based meta-heuristic OA, motivated by the social behaviour of birds' flocking, herding of tetrapod's, and the shoaling and schooling of fish [2,11,48,51,60]. More precisely, swarm behaviour is the collective motion of many self-propelled entities, called a 'swarm', in the field of optimization. PSO is used to optimize a problem by considering a population of candidate solutions called 'particles', which move around in a definite search space to find the nearest optimal solution, and shows decent performance on the global and local search. The movement of the particles can be adjusted by using a deterministic and a stochastic component. In the search space, each particle is influenced by its 'best' achieved position (called personal best) and the

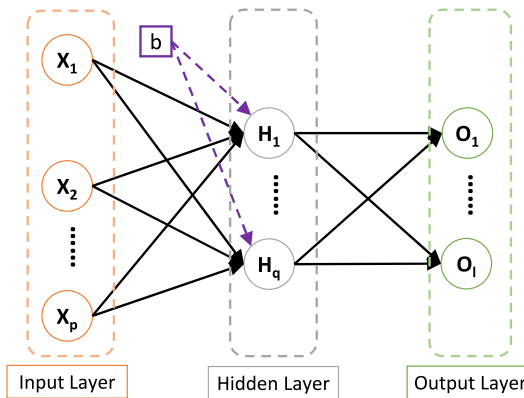


Fig. 1. A general structure of ELM.

group ‘best’ position (called global best), but tends to move randomly. For a particle i with M -dimensional position vector $x_i = (x_{i1}, x_{i2}, x_{i3}, \dots, x_{iM})$ and velocity vector $v_i = (v_{i1}, v_{i2}, v_{i3}, \dots, v_{iM})$, $i = \{1, 2, 3, \dots, m\}$ (m = number of particles) at each iteration, each particle/swarm changes its position. Accordingly, the new velocity and position of the particle are given by:

$$v_i^{t+1} = w \times v_i^t + c_1 \cdot r_1 (x_{best_i}^t - x_i^t) + c_2 \cdot r_2 (g_{best}^t - x_i^t) \quad (4)$$

$$x_i^{t+1} = x_i^t + v_i^{t+1} \cdot t \quad (5)$$

where w is the inertia weight with a decreasing pattern given by:

$$w = w_{max} - [(w_{max} - w_{min}) \times t/k] \quad (6)$$

where w_{min} and w_{max} are the minimum and maximum inertia weights; t represents the current iteration number; and k represents the maximum number of iterations. In Eq. (4), c_1 , r_1 , c_2 , and r_2 are the first positive constant, first random parameter, second positive constant, and second random parameter, respectively; x_{best} and g_{best} denote the position of personal best and global best, respectively. It is assumed that the random parameters (r_1 , r_2) are uniformly distributed numbers within (0,1). The particles try to unite to search for an optimal solution in line with the fitness function. The modern application of this swarm intelligence technique is becoming very popular and has been applied successfully in different fields of engineering for optimization, training of different ML algorithm [32,33,33,34,36–39,41–46,49,52,61–63], and other areas as well.

2.3. Modified Particle Swarm Optimization (MPSO)

Searching of global minimum remains a burdensome task in all minimization problems. Thus, an extended study on the acceleration parameters was performed by Kennedy in 1998. Normally, during the early stages of the optimization in population-based meta-heuristic algorithms, it is desirable to encourage the individuals (or particles) to explore the entire search space without assembling in and around local optima, while in subsequent stages, it is essential to improve convergence toward the global minimum to find the optimal solution efficiently. Proper fine-tuning of the acceleration coefficients (c_1 and c_2) may result in faster convergence and assuagement of local minima. Considering these facts, Bao and Mao [50] proposed a modified version of PSO (MPSO) to enhance the global search in the primary stage of optimization and to encourage the particles to converge toward the global optima in the subsequent stage of the search. In this process, the cognitive component (c_1) can be reduced, while the social component (c_2) is increased by changing the values of c_1

and c_2 . In addition, the rates of slopes of c_1 and c_2 are used to control the particles movement. At the beginning, small c_2 and large c_1 are used, and particles are allowed to move around the search space rather than moving toward the population best. At the same time, the opposite arrangement of c_2 and c_1 allows the particles to converge to the global optimum in the subsequent step. In MPSO, the modified acceleration coefficients can be expressed as follows:

$$c_1 = c_{1max} - \frac{t(c_{1max} - c_{1min})}{k} \quad (7)$$

$$c_2 = c_{2min} + \frac{t(c_{2max} - c_{2min})}{k} \quad (8)$$

where t and k are the present and maximum iterations, respectively. Bao and Mao [50] proposed five different cases of time-varying acceleration coefficients (4 asymmetrical and 1 symmetrical) with different falling rates of c_1 and rising rates of c_2 . The maximum value of 3.00 for c_1 and c_2 and the minimum value of 0.50 for c_1 and c_2 were considered by the authors. Based on the simulations results, the authors suggest that the convergence rate of MPSO is faster than that of the SPSO, which means MPSO is capable of escaping from the areas of local minima by incorporating the global minimum effectively. Bao and Mao [50] also showed that time-varying acceleration coefficients, i.e. $c_1 = 2.25 - 1.25$ and $c_2 = 0.50 - 2.55$, can result in stable convergence to a high-quality solution in the early iterations (about 150 iterations) and, thus, the best probability of success for the optimization. The detailed configurations of MPSO used in ELM-MPSO modelling are presented in the results and discussion section.

2.4. PSO with Time-varying Acceleration Coefficients (TPSO)

In SPSO, during the initial stages of the optimization process, it is desirable to encourage the individuals to explore the entire search space without coinciding around the local optima. In contrast, to find the optimum solution efficiently in the later stages, it is important to enhance the convergence towards the global optimum. Thus, Tang and Zhang [53] proposed time-varying acceleration coefficients to enhance the global search in the initial stage of the optimization process and encourage the particles to congregate to the global optimum at the end. The acceleration coefficients (c_1 and c_2) with time-varying expressions proposed by Tang and Zhang [53] are given by:

$$c_1 = c_{min} + (c_{max} - c_{min}) \cdot \exp \left(- \left(\frac{4t}{k} \right)^2 \right) \quad (9)$$

$$c_2 = c_{max} - (c_{max} - c_{min}) \cdot \exp \left(- \left(\frac{4t}{k} \right)^2 \right) \quad (10)$$

In the aforementioned development, c_1 is reduced with the passage of time, while c_2 is increased simultaneously. With larger c_1 and smaller c_2 in the initial stage, the particles are allowed to roam around the search space instead of moving towards the population best. Later, smaller c_1 and larger c_2 allow the particles to congregate to the global optima. Tang and Zhang [53] proposed separate values of c_{max} and c_{min} as 2.50 and 0.50, respectively, in their study. The simulations show that TPSO provides a better probability of finding global optimum and mean best value than other algorithms.

2.5. Improved Particle Swarm Optimization (IPSO)

In order to determine the region of global optimum of a multi-dimensional optimization problem in the early stage, PSO initiates an approximate search in the solution space, while in

the second stage, the algorithm will search the local search so that the global optimum can be found as soon as possible. From this frame of reference, in the early stage, the cognitive coefficient (c_1) should be changed very acutely for an effective global search, whereas c_1 should be decreased as calmly as possible to maintain an effective local search. In this theory, the main concern is how to decrease c_1 so that a balance between exploration and exploitation can be maintained. To achieve this, Cui et al. [48] proposed three non-linear functions with time-varying c_1 , the mathematical expressions for which are the upwards function in Eq. (11), concave function in Eq. (12), and exponential function in Eq. (13):

$$c_1(t) = c_{1max} + (c_{1max} - c_{1min}) \cdot \left(\frac{t}{k}\right)^2 \quad (11)$$

$$c_1(t) = c_{1max} + (c_{1max} - c_{1min}) \cdot \left(\frac{t}{k}\right)^2 - (c_{1max} - c_{1min}) \cdot \left(\frac{2t}{k}\right) \quad (12)$$

$$c_1(t) = c_{1min} + \left(\frac{c_{1max}}{c_{1min}}\right)^{\frac{1}{1+10 \times \frac{t}{k}}} \quad (13)$$

where t is the current iteration; k is the total number of iterations; and c_{1max} and c_{1min} denote the upper and lower bound of the c_1 , respectively. On the other hand, the adjustment of c_2 as per [64] is given by:

$$c_2 = 3.0 - c_1 \quad (14)$$

where the sum of the accelerator coefficients is considered as 3.0 ($c_1 + c_2 = 3.0$). As both the acceleration coefficients change dynamically in a non-linear manner, the improved PSO (IPSO) with time-varying accelerator coefficients is defined. The authors of [48] suggest that the concave function (i.e. second strategy) with $c_{1max} = 2.50$ and $c_{1min} = 0.50$ is the best choice among the three strategies for multi-modal numerical optimization problems.

2.6. Brief overview of GWO, SMA and HHO

GWO, SMA, and HHO are categorized as population-based meta-heuristic algorithms, which mostly mimic the social behaviour of swarms, flocks, or schools of creatures in nature [65]. These algorithms are also called swarm intelligence OAs. The working principle of these algorithms is almost similar to physics-based algorithms, but the search agents navigate using the simulated collective and social intelligence of creatures.

In GWO, the social behaviour of grey wolves has been modelled. Grey wolves, which belong to the Canidae family, are considered apex predators. GWO comprises a mechanism of how grey wolves catch their prey and their leadership hierarchy. To simulate the hierarchy system in the model, four types of grey wolves are taken in each wolf pack. Alpha (α) wolf is the leader and the most responsible followed by Beta (β) wolves and Delta (δ) wolves. Omega (ω) wolves are the lowest in the hierarchy and least responsible.

SMA is basically a stochastic optimizer, proposed based upon the oscillation mode of slime mould in nature. This algorithm has many features that simulate the behaviour and morphological changes of slime mould Physarum polycephalum in foraging and does not model its complete life cycle. It also uses adaptive weights to simulate positive and negative feedback.

HHO is a population-based gradient-free OA, inspired by the behaviour of the Harris hawks birds in nature. The nature of the algorithm is based on the collaboration between hawks in chasing and hunting the prey. According to the HHO algorithm, a group of hawks attempt to collaboratively strike from various directions

and at the same time converge on an identified prey to hunt it by surprise. Harris' hawks display a range of chasing techniques according to the diverse nature of the circumstances and a prey's escape patterns. One of the superiorities of the HHO algorithm is its applicability to constrained problems. In addition, as a global optimizer, HHO is able to keep the balance between the phases of exploitation and exploration as well.

The detailed working principle of these swarm intelligence OAs can be obtained from Mirjalili et al. [66] for GWO, Li et al. [67] for SMA, and Heidari et al. [65] for HHO.

2.7. Brief overview of ANN, GP, SVM and GMDH

ANN is the piece of a computing system, designed to simulate the way the brain of human beings analyses and processes information. It is one of the widely used soft computing techniques and is known as the foundation of ML. An ANN is consisting of three layers, namely the input layer, hidden layer(s), and output layer, which are interconnected through links, called weights. Each layer contains one or more neurons working as an independent processing element. In ANNs, the learning function is used for initialization, training, and adaptation. During the course of the training process, ANN is continuously updated by a training function, which repeatedly applies the input dataset till the desired error criterion is obtained. Different training functions, such as *trainlm* (Levenberg–Marquardt backpropagation), *traingb* (Conjugate gradient with Powell/Beale restarts), *traincgp* (Conjugate gradient backpropagation with Polak–Ribiére updates), and *trainbr* (Bayesian regularization backpropagation) are normally used in ANN modelling.

GP, an extension of genetic algorithms, is a symbolic optimization technique that creates computer programs to solve non-linear problems. The principle of Darwinian natural selection is used to solve a problem [68,69]. In GP, a random population of individuals, i.e., a set of computer programs, is created to attain high multiplicity. A population member is a hierarchically arranged tree comprising functions and terminals. Generally, the function set contains arithmetic operators (+, −, ×, ÷, etc.), trigonometric functions (\sin , \cos , \tan , \tanh , etc.), Boolean operators (AND, OR, NAND, NOR, etc.), or any other mathematical operators, while the terminal set comprises arguments, variables, logical constants, numerical constants, etc. These functions and terminals are selected randomly from sets of functions and terminals, and constructed together to form a computer model. To obtain higher predictive accuracy, different parameters, such as population size, tournament size, maximum number of generations, maximum number of genes, crossover and mutation probability, and functions are tuned.

SVM is a supervised ML algorithm that analyses data for regression and classification problems. Basically, SVM was designed to find out the solution of complex functions or patterns with good generalization ability. It can solve linear and non-linear problems and works well for many practical problems. In SVM, samples selected for training are called support vectors. The optimal separation of the data is initiated by the support vector's optimal separation. In general, two basic parameters, namely sigma and gamma, and kernel function play an important role in SVM modelling. The commonly used kernel functions are linear, sigmoid, and radial basis function.

GMDH [70–72] is a self-organizing approach based on evaluating the performance of multiple-input and single-output data pairs. The main function of the GMDH network is actually to construct a function in a feed-forward network based on a second-degree transfer function. In this algorithm, the number of the

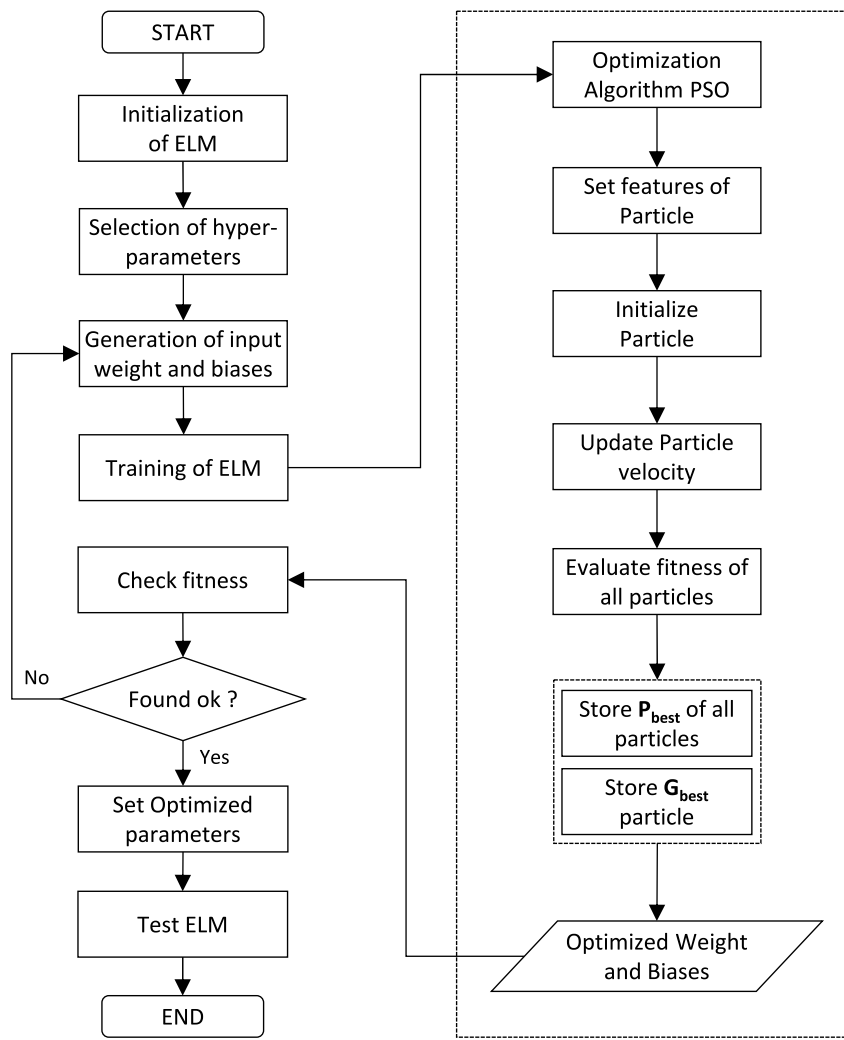


Fig. 2. Flow chart showing the steps in developing the ELM-PSO model.

hidden layers, hidden neurons, the number of effective input variables, and the optimal model structure are automatically determined. The mapping between input and output is done through a GMDH neural network, which is a non-linear function called the Volterra series [73]. The unknown coefficients in the Volterra series are solved using regression methods based on the principle of least square [73].

The detailed theoretical background of these CSC algorithms and their successful application in different engineering fields can be found in the literature [3,12,14,30,68,69].

2.8. Hybridization of ELM-based meta-heuristic models

As stated above, ELM has two learning parameters (hidden weights and hidden biases), which are selected randomly to generate the output weights. In addition, it has two hyper-parameters, namely the number of hidden neurons (N_h) and activation function, that play an essential role in ELM modelling. Note that the optimum values of N_h and the activation function can be easily obtained by a trial-and-error approach for a particular problem. However, it is challenging to generate the optimum values of hidden weights and biases for the same problem. Therefore, it is desirable to obtain the optimum values of learning parameters for predicting the desired output more accurately. For this purpose, OAs were used to optimize the learning parameters of ELM in ELM-based modelling.

The methodological development of the ELM-PSO model can be described as follows: (1) selection of hyper-parameters (N_h and activation function); (2) random generation of learning parameters; (3) training of ELM using the training dataset; (4) implementation of PSO; (6) iterative generation of weights and biases using PSO; (7) check fitness at each iteration; (8) generation of optimized values of learning parameters based on iterative performance; and (9) finally, validation of the ELM-PSO model using optimized weights and biases. The same procedure was followed for the ELM-MPSO, ELM-TPSO, ELM-IPSO, ELM-GWO, ELM-SMA, and ELM-HHO models; however, the parametric configurations of the acceleration coefficient for MPSO, TPSO, and IPSO were selected according to the methodologies stated above. Although the procedures for developing the hybrid models are same, the values of the optimized weights and biases of the developed models are different. A flow chart indicating the steps in developing the ELM-PSO model is presented in Fig. 2.

3. Study area

The Ministry of Indian Railways has planned to build a 10,122-km long [74] Dedicated Freight Corridor (DFC) under the Golden Quadrilateral Freight Corridor (GQFC) project solely for carrying freight. GQFC has six DFCs, of which two corridors, namely Western Dedicated Freight Corridor (WDFC) and Eastern Dedicated Freight Corridor (EDFC), have already been implemented and are

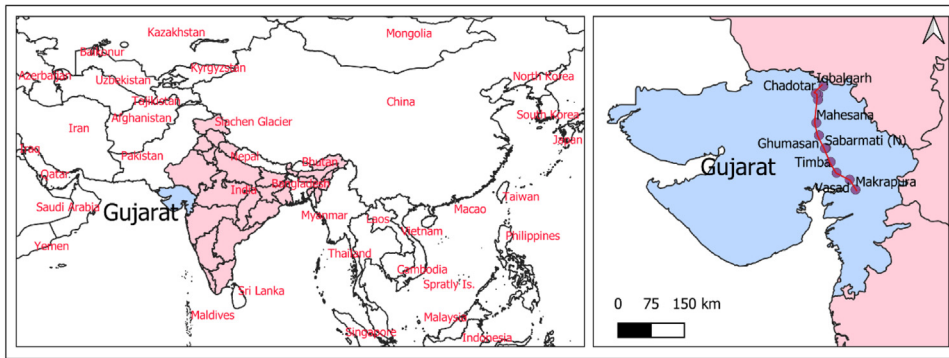


Fig. 3. Geographical layout of 'Iqbalgarh-Vadodara' section.

under construction at the time of this writing. In this work, a section of the WDFFC (Iqbalgarh-Vadodara section) was chosen as the study area, which is 308 km long (revised length of 340 km) and will pass through the states of Gujarat, India. From the project, a total of 312 test data results of soaked CBR (as per IS: 2720 (Part 16) - 1987) was collected, including gravel content (G), the content of sand (S), silt and clay (S&C) content along with PI, maximum dry density (MDD), OMC, and CBR values of the sub-soil of this section. A geographical layout of the study area is shown in Fig. 3.

4. Data processing and analysis

4.1. Descriptive statistics and statistical visualization

In order to develop the predictive models, a total of 312 test data points of soaked CBR (IS: 2720 (Part 16) - 1987) along with 6 basic soil properties (G, S, S&C PI, MDD, and OMC) of 5 different soils, namely CL, CI, SC, ML and SM (the abbreviations have their own meaning) were collected. The basic soil properties of 5 different soils were considered as input variables in the predictive models. Table 1 presents the descriptive statistics of the soil parameters, including the CBR of soils. For a more detailed understanding, descriptive statistics with the minimum, average, and maximum values of each parameter for each soil are presented in Table 2. In Tables 1 and 2, it is seen that the CBR of soil ranges from 5.20 to 10.20, indicating that a wide range of experimental data is available in the database. The range of other soil parameters can also be observed in Table 2 separately for each soil. As can be seen, most soils possess a sand content between 10% and 80%, while the S&C content in the soils lies in the range of 6% to 80%. Two soils (ML and SM) have no plasticity, while the other soils show plasticity in the range of 15% to 20%. The values of OMC and MDD are in the ranges of 7%–15% and 1.77–2.05 g/cm³, respectively.

To visualize the interrelationship between the soil parameters, graphical representations are presented in Fig. 4(a-b) in the form of a correlation matrix and 2-D density plot, which display the collinearity (based on Pearson correlation coefficient) between the soil parameters and their ranges. As can be seen, the parameters S, S&C, PI, MDD and OMC strongly correlate to the CBR, in which S&C, PI, and OMC have *-ve* correlation. However, little correlation is observed among the other soil parameters. Linear trends between the soil parameters and CBR are shown in Fig. 5(a-f) for all soils, from which the amount of collinearity between the soil parameters can also be established.

4.2. AI-based analysis

In the field of soft computing, it is recommended that the values of processing variables be normalized within a predefined range to enhance the computational efficiency in establishing the relation between response and predicted variables. On this note, a '*min-max*' normalization technique was used in this study [45, 62,75]. Using the expression given in Eq. (15), the main dataset was normalized between 0 and 1.

$$x_{\text{norm}} = (x - x_{\min}) / (x_{\max} - x_{\min}) \quad (15)$$

where x is the actual value; and x_{\min} and x_{\max} are the minimum and maximum values of the measured variables, respectively. After normalization, the main dataset (312 instances) was apportioned into training and testing datasets. The idea behind the extraction of the testing dataset is to check the performance of the trained model with a new set of data. For this purpose, 80% of the main dataset (250 experimental results) was selected randomly as the training dataset, while the remaining dataset, i.e., testing dataset (62 experimental results) was used to validate the developed models. Although no thumb rule or specific criteria are available for the dataset (number of instances) to be used in a predictive model, the researchers' choice will mainly depend on the type of problem at hand. Generally, a model constructed with a large dataset can be considered more reliable than that performed with a limited number of samples. Also, a predictive model with a greater accuracy level derived from studying a large number of samples in the validation stage is more reliable. In this study, 20% of the main dataset, i.e., 62 observations, was considered to validate the developed models.

In the present study, k-fold ($k = 5$) cross-validation was followed to select the most significant training and testing datasets. In the k-fold cross-validation, the sample is randomly partitioned into k equal subsets. Among these subsets, a single subset was selected as the testing dataset, while the remaining subsets was used as the training dataset. The idea behind the implementation of k-fold cross-validation was to construct the model more effectively so that the highest prediction accuracy can be achieved in the validation phase.

Subsequently, to assess the performance of the developed models, widely used performance indices [76–84], viz., determination coefficient (R^2), variance account for (VAF), performance index (PI), Willmott's index of agreement (WI), mean absolute error (MAE), mean absolute percentage error (MAPE), mean bias error (MBE), and root mean square error (RMSE) were determined. The mathematical expressions of these indices are given by:

$$R^2 = \frac{\sum_{i=1}^n (y_i - \bar{y}_i)^2 - \sum_{i=1}^n (y_i - \tilde{y}_i)^2}{\sum_{i=1}^n (y_i - \bar{y}_i)^2} \quad (16)$$

Table 1
Statistical details of all soil parameters.

Statistical param.	G	S	S&C	PI	MDD	OMC	CBR
Minimum	0.00	9.00	6.00	0.00	1.77	7.10	5.20
1st quartile	0.00	36.00	32.00	0.00	1.85	7.70	7.50
Median	0.00	56.00	42.00	0.00	1.91	7.95	8.50
Mean	1.82	51.60	46.58	5.14	1.90	9.32	8.35
3rd quartile	0.00	67.00	61.00	14.00	1.92	11.50	9.10
Maximum	30.00	84.00	91.00	26.00	2.05	15.80	10.20
Standard error	0.24	1.04	1.03	0.43	0.00	0.13	0.06
Standard deviation	4.22	18.39	18.20	7.59	0.06	2.23	1.09
Variance	17.83	338.21	331.22	57.55	0.00	4.99	1.18
Skewness	3.00	-0.42	0.40	0.88	0.07	1.03	-0.53
Kurtosis	13.35	1.99	2.17	1.98	2.50	2.89	2.87

Table 2
Soil classification wise statistical details.

Soil classification	Param.	G	S	S&C	PI	MDD	OMC	CBR
CL	Min	0.00	9.00	50.00	11.00	1.77	8.80	5.50
	Mean	2.99	30.00	67.33	15.39	1.84	12.10	7.19
	Max	17.00	82.00	91.00	19.00	1.91	15.50	9.10
CI	Min	0.00	17.00	56.00	19.00	1.77	8.30	5.20
	Mean	1.55	27.00	71.55	20.91	1.82	14.55	6.03
	Max	8.00	38.00	83.00	26.00	1.98	15.80	9.90
SC	Min	0.00	49.00	20.00	12.00	1.85	8.50	8.00
	Mean	2.38	55.00	42.63	14.13	1.89	10.28	8.69
	Max	14.00	75.00	49.00	18.00	1.92	12.70	9.20
ML	Min	0.00	18.00	51.00	0.00	1.81	7.50	7.10
	Mean	0.00	36.00	64.09	0.00	1.88	8.82	8.09
	Max	0.00	49.00	82.00	0.00	1.95	9.90	8.80
SM	Min	0.00	41.00	6.00	0.00	1.81	7.10	7.80
	Mean	1.53	64.00	34.10	0.00	1.93	7.82	9.02
	Max	30.00	84.00	59.00	0.00	2.05	11.10	10.20

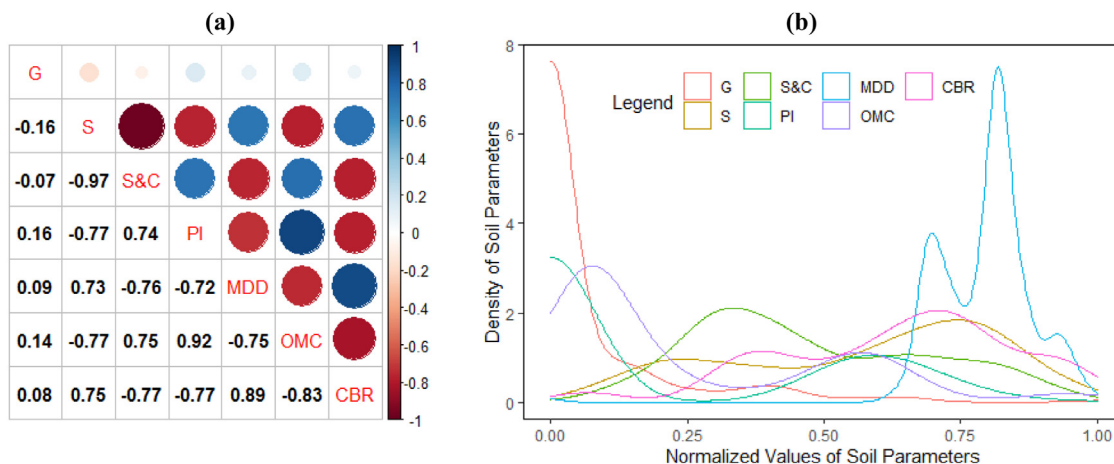


Fig. 4. (a) Correlation matrix and (b) 2-D density plot of the soil parameters.

$$VAF = \left(1 - \frac{\text{var}(y_i - \tilde{y}_i)}{\text{var}(y_i)} \right) \times 100$$

$$PI = adj \cdot R^2 + (0.01 \times VAF) - RMSE$$

$$WI = 1 - \left[\frac{\sum_{i=1}^n (y_i - \tilde{y}_i)^2}{\sum_{i=1}^n \{ |\tilde{y}_i - y_{avg}| + |y_i - y_{avg}| \}^2} \right]$$

$$MAE = \frac{1}{n} \sum_{i=1}^n |(\tilde{y}_i - y_i)|$$

$$MAPE = \frac{1}{n} \sum_{i=1}^n \left| \frac{y_i - \tilde{y}_i}{y_i} \right| \times 100$$

$$(17) \quad MBE = \frac{1}{n} \sum_{i=1}^n (\tilde{y}_i - y_i) \quad (22)$$

$$(18) \quad (19) \quad RMSE = \sqrt{\frac{1}{n} \sum_{i=1}^n (y_i - \tilde{y}_i)^2} \quad (23)$$

where y_i and \tilde{y}_i are the experimental and predicted i^{th} value; n is the number of samples in a dataset, i.e., the number of test results under consideration; and y_{avg} is the mean of the actual values. Note that for a predictive model with 100% accuracy, the value of these parameters should be equal to their ideal values (presented in Table 3). Among the eight parameters, the first four parameters (R^2 , VAF , PI , and WI) were used to measure the trend of the predictive models, while MAE , $MAPE$, MBE , and $RMSE$ were

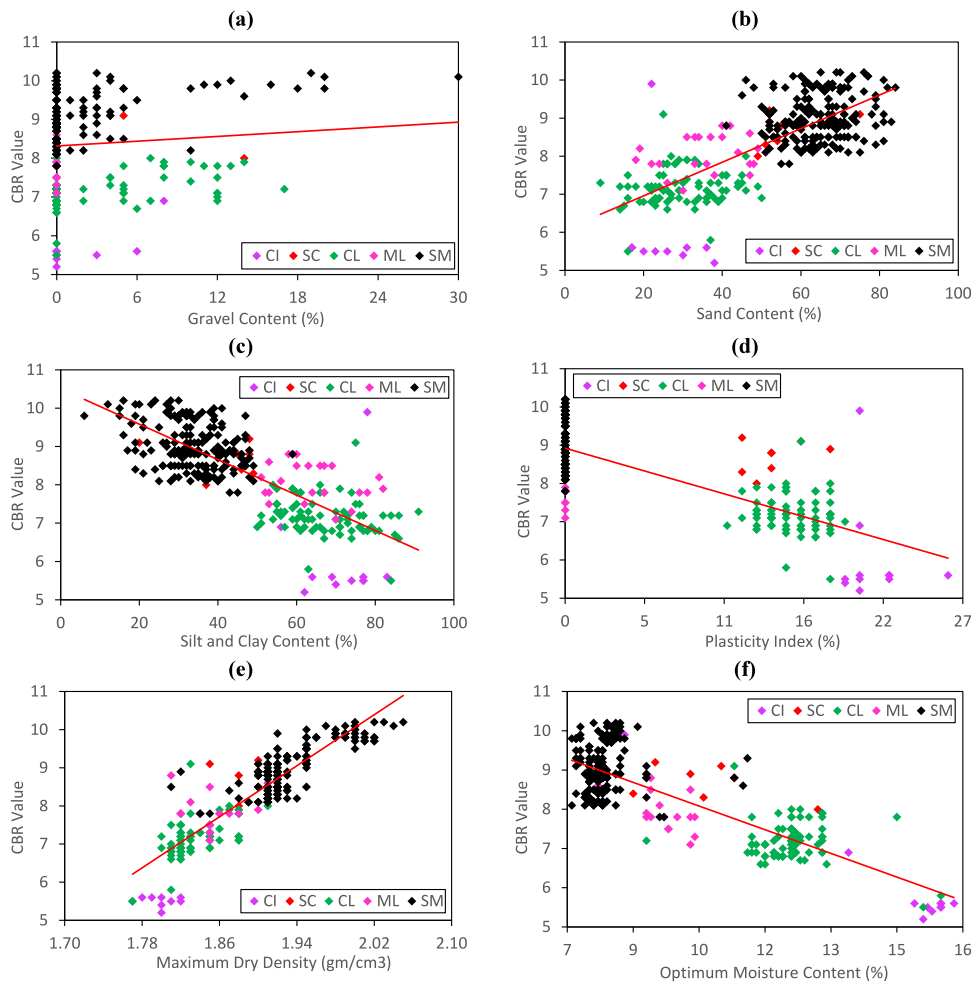


Fig. 5. Linear behaviour of CBR with (a) gravel content, (b) sand content, (c) silt and clay content, (d) plasticity index, (e) maximum dry density, and (f) optimum moisture content.

Table 3
Ideal value of different performance indices.

Parameters	Ideal value	Parameters	Ideal value
R^2	1	MAE	0
VAF	100	MAPE	0
PI	2	MBE	0
WI	1	RMSE	0

used to measure the amount of error associated with the predictive models. The reason behind the selection of these indices was to assess the performance of the developed models from different aspects, such as the degree of correlation, variances, and associated error between the experimental and predicted values.

In addition to the indices mentioned above, a novel engineering index is proposed in line with the concept introduced by Duan et al. [85]. However, this index was re-defined in the present study as the Accuracy index (A_{10}), which can be very useful to calculate the amount of theoretical error associated with a predictive model. The mathematical expression of A_{10} is given by:

$$A_{10} = \frac{a_{10}}{n} \quad (24)$$

where n denotes the total number of samples; and a_{10} represents the number of samples with a ratio of the experimental value to predicted value falling between 0.90 and 1.10. It is important to note that for an ideal predictive model, the value of A_{10} is

expected to be 1 or 100%. The physical interpretation of this engineering index declares the number of samples that satisfies predicted values with a $\pm 10\%$ deviation of the experimental or actual values. Usually, a $\pm 10\%$ error is normally acceptable while making predictions in the field of geotechnical engineering. Therefore, A_{10} is an index that perfectly captures this idea and suitably represents the accuracy of the predicted results. However, a prediction error beyond 10% is always undesirable and would render the developed model inefficient. The deviation of A_{10} from its ideal value would also reflect the inaccuracy of the developed model.

5. Results and discussion

In this section, the outcomes of the proposed models in predicting the soaked CBR are evaluated in detail. As mentioned earlier, six soil parameters, namely G, S, S&C, PI, MDD, and OMC, were considered as input variables to predict the CBR of soil in soaked conditions. For this purpose, a total of 312 experimental results of soaked CBR were collected from an ongoing project of DFC. In the first stage, the training dataset was used to develop the predictive models, and subsequently, the performance of the developed models was assessed based on validation datasets. Eight performance indices were calculated to estimate the accuracy of the developed models from different aspects.

Furthermore, the generalization capabilities and robustness of the developed models were assessed for the new datasets.

Table 4
Configuration of optimization parameters in ELM-based modelling.

Parameters	PSO	MPSO	TPSO	IPSO	GWO	SMA	HHO
n_s	30	30	30	30	30	30	30
v	Eq. (4)	Eq. (4)	Eq. (4)	Eq. (4)	-	-	-
c_1	1	Eq. (25)	Eq. (27)	Eq. (29)	-	-	-
c_2	2	Eq. (26)	Eq. (28)	Eq. (30)	-	-	-
N_h	18	14	14	15	12	21	17
k	200	200	200	200	200	200	200
Cost function	RMSE	RMSE	RMSE	RMSE	RMSE	RMSE	RMSE

It is pertinent to mention that a model with higher predictive accuracy in the validation phase should be considered as reliable. Therefore, to validate the proposed models, three-level validations are adopted in the present study based on three datasets: (1) the unused dataset, i.e., testing dataset (selected based on k-fold cross-validation); (2) the experimental database obtained from 40 new experiments performed in the geotechnical engineering laboratory of National Institute of Technology Patna; and (3) the simulated datasets. The experiments were performed in the geotechnical laboratory to generate new experimental datasets, specifically for the validation of the proposed models. A detailed comparison of the accuracies of the developed models is also presented. In the end, uncertainty analysis and statistical testing were performed to assess the overall performance of the developed models.

5.1. Configuration and realization of ELM-based models

As mentioned earlier, to determine the ELM structure, it is necessary to first specify its hyper-parameters (N_h and activation function). In the present study, N_h varying from 5 to 50 was investigated with a sigmoid activation function to identify the optimum configuration of the ELM model. Following the trial-and-error approach, the most suitable value (based on the result of the testing dataset) of N_h was obtained as 15.

In the subsequent stage, the optimum number of N_h for the ELM-based ANSI models and ELM-GWO, ELM-SMA, and ELM-HHO were investigated in the range of 5 to 50. The deterministic parameters, such as swarm size (n_s) and the maximum number of iteration (k), were kept constant throughout the analysis for a fair comparison. The most effective choice of these parameters was obtained by configuring them (via the trial-and-error approach) within a suitable range, and their optimum values for the proposed optimization models are given in Table 4. The detailed procedure of ELM-PSO, including the ELM-MPSO, ELM-TPSO, ELM-IPSO, ELM-GWO, ELM-SMA, and ELM-HHO models performed for predicting the CBR of soils, are discussed below.

In ELM-PSO modelling, ELM was first initialized, then PSO was used to optimize the learning parameters of ELM. When training the ELM-PSO model was accomplished, the ultimate structure of the model was finalized. Note that, the PSO optimized ELM model includes 6 input neurons, 18 hidden neurons, and 1 output neuron. In ELM-PSO, the number of optimized weights and biases are 126 (i.e., $18 \times 6 + 18$). Moreover, during the course of optimization, the sigmoid function and RMSE were used as the activation function and cost function, respectively. The search for global optimum was performed in 200 iterations (i.e., $k = 200$) with $n_s = 30$, $w_{max} = 0.9$, $w_{min} = 0.4$, $c_1 = 1$, and $c_2 = 2$, and the optimized values of weights and biases were generated to train and validate the model.

Analogous to the ELM-PSO model, the ELM-MPSO, ELM-TPSO, and ELM-IPSO models were constructed and the values of the deterministic parameters (n_s , w_{max} , w_{min} , and k) were kept constant for all the models during the course of optimization. The optimum number of N_h were investigated in the range of 5 to 50 for each model separately. However, in ELM-MPSO modelling,

the maximum and minimum values of c_1 and c_2 were set as (2.55 and 0.5) and (2.25 and 1.25), respectively. Therefore, the resulting expressions of the acceleration coefficients are given by:

$$c_1 = 2.55 - \frac{t(2.55 - 0.50)}{k} \quad (25)$$

$$c_2 = 1.25 + \frac{t(2.25 - 1.25)}{k} \quad (26)$$

To update the values of c_1 and c_2 in each iteration, the acceleration coefficients with time-varying expressions were modelled in ELM-TPSO using $c_{max} = 2.50$ and $c_{min} = 0.50$. Consequently, the resulting expressions for the time-varying acceleration coefficients were obtained as:

$$c_1 = 0.50 + (2.50 - 0.50) \cdot \exp\left(-\left(\frac{4t}{k}\right)^2\right) \quad (27)$$

$$c_2 = 2.50 - (2.50 - 0.50) \cdot \exp\left(-\left(\frac{4t}{k}\right)^2\right) \quad (28)$$

In contrast, to tune the acceleration coefficients in the ELM-IPSO model, the concave function was modelled with $c_{max} = 2.50$ and $c_{min} = 0.50$. Therefore, the resulting expressions of the equation givens in Eqs. (12) and (14) can be written as:

$$c_1 = 2.50 + (2.50 - 0.50) \cdot \left(\frac{t}{k}\right)^2 - (2.50 - 0.50) \cdot \left(\frac{2t}{k}\right) \quad (29)$$

$$c_2 = 3.0 - c_1 \quad (30)$$

Based on the optimum values of N_h (refer to Table 4), the number of optimized weights and biases are 98 for ELM-MPSO ($N_h = 14$), 98 for ELM-TPSO ($N_h = 14$), and 105 for ELM-IPSO ($N_h = 15$) models. The same procedure was followed for other ELM-based meta-heuristic models and the number of optimized weights and biases were obtained as 84 for ELM-GWO ($N_h = 12$), 147 for ELM-SMA ($N_h = 21$), and 119 for ELM-HHO ($N_h = 17$) models. Note that although the procedures of meta-heuristic optimized models are the same, the values of the optimized weights and biases of the developed models are different for all cases. Furthermore, the convergence curves of the ELM-PSO model, including other ELM-based meta-heuristic models are presented in Fig. 6. It is pertinent to mention that the convergence behaviour of any OA is very important in evaluating its performance as it indicates the ability to escape from local optima. Moreover, an OA facing an uneven exploration and exploitation dilemma is more prone to get stuck in local optima. As can be seen, ELM-MPSO achieved a superior solution faster (less than 70 iterations) than other employed models, confirming the superiority of the MPSO algorithm in ELM-MPSO modelling.

Note that, all the ELM-based models employed in this study were constructed in a MATLAB environment, and run in MATLAB 2015a version with i7-4790U CPU @ 3.60 GHz, 8.00 GB RAM system configuration. The computation costs for 200 iterations were noted as ELM-PSO=18.461010 s, ELM-MPSO=17.719746 s, ELM-TPSO=17.799294 s, ELM-IPSO=18.955517 s, ELM-GWO=17.980727 s, ELM-SMA=27.699426 s, and ELM-HHO=22.357501 s, which indicates the proposed ELM-MPSO attained the desired prediction

Table 5
Details of performance indices for the training dataset.

Models	Performance indices							
	R ²	VAF	PI	WI	MAE	MAPE	MBE	RMSE
ELM-PSO	0.8986	89.86	1.7255	0.9731	0.0530	11.3770	-0.0002	0.0684
ELM-MPSO	0.9100	91.00	1.7525	0.9763	0.0498	10.6483	-0.0001	0.0645
ELM-TPSO	0.9029	90.29	1.7355	0.9743	0.0509	10.5538	0.0000	0.0670
ELM-IPSO	0.8986	89.86	1.7254	0.9731	0.0538	11.3863	0.0000	0.0685
ELM-GWO	0.9043	90.43	1.7388	0.9746	0.0527	10.8116	0.0000	0.0665
ELM-SMA	0.8930	89.30	1.7122	0.9714	0.0550	11.3170	0.0000	0.0703
ELM-HHO	0.9062	90.62	1.7435	0.9752	0.0508	10.6354	0.0000	0.0658
ELM	0.8464	84.64	1.6033	0.9577	0.0643	14.0912	-0.0006	0.0843
ANN	0.8564	85.64	1.6265	0.9605	0.0607	17.0481	0.0000	0.0815
GP	0.8736	87.36	1.6665	0.9658	0.0584	11.7000	-0.0001	0.0764
SVM	0.8712	87.10	1.6607	0.9654	0.0580	11.9004	-0.0015	0.0772
GMDH	0.8653	86.52	1.6470	0.9635	0.0622	12.3267	-0.0040	0.0790

accuracy with very less computational cost. To better demonstrate the performance of proposed meta-heuristic optimized models, the performance was compared to those of conventional ELM and ANN, GP, SVM, and GMDH models, the details of which are presented in the following sub-section.

5.2. Configuration and realization of CSC models

To train the conventional ANN, *trainlm*, i.e., Levenberg–Marquardt backpropagation function was used as the activation function. The structure of the developed ANN includes 6 input neurons, 8 hidden neurons, and 1 output neuron. During the course of training of ANN algorithm, 20% of the training dataset was used to stop the overfitting. The terminating criteria for the final GP model are population size=400, number of generations=200, tournament size=20, number of genes=6, maximum tree depth=4, and mutational probability=0.80. On the other hand, to establish the optimum SVM model, the values of hyperparameters ‘gamma’ and ‘C’ were selected in the range of 0.1 to 200 and 0.001 to 0.1, respectively, using the radial basis function as the kernel function. And, the most suitable structure of GMDH consists of 4 hidden layers with 10 neurons in each layer. The best performance was achieved when the number of hidden layers was set to 4. It may be noted that, to establish the employed CSC models, a trial-and-error approach was followed, and the best performing model was selected based on the performance of the testing dataset. For this purpose, 5-fold cross-validation was considered in each case.

In the following sub-section, the outcomes of the proposed models are presented in detail based on several performance parameters. Visual representations of the predictive results in the form of Taylor diagrams and Accuracy matrix are also presented and discussed.

5.3. Performance of the employed models

This sub-section presents a comparative assessment of the proposed models in terms of their accuracies. Several performance indices of the developed model were determined for the training dataset and are presented in Table 5. In particular, the 8 performance indices presented in Section 4.2 were calculated for the employed models. The analysis yielded accuracy levels in the range of 84.64% ($R^2 = 0.8464$) to 91.00% ($R^2 = 0.9100$) in terms of R^2 , while the values of RMSE were obtained in the range of 6.45% ($RMSE = 0.0645$) to 8.43% ($RMSE = 0.0843$) for the developed models. It may be noted that the values of R^2 greater than 80% indicate that the proposed models obtained a good fit to the experimental dataset. Also, the values of performance indices show that there is no uncertainty between the results, as all the parameters follow the desired trends. Neither any large variation nor any unacceptable values were obtained in this phase.

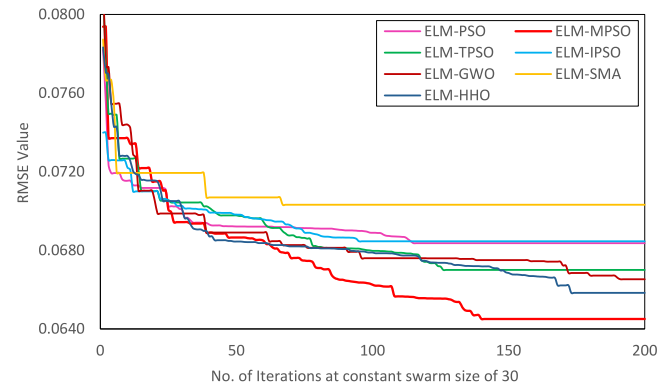


Fig. 6. Convergence behaviour of ELM-based models.

In the training stage, the ELM-MPSO model outperformed the other models. The ELM-TPSO was found to be the second-best model among the ELM-based ANSI models. Overall, the ELM-HHO model was found to be the second-best model, followed by other ELM-based models and CSC models (refer to Table 5). The predictive results of the ELM-based models for predicting the soaked CBR are illustrated in Fig. 7(a–n), while the predictive results of the classical ELM and ANN, GP, SVM, and GMDH models are shown in Fig. 7(o–x) in the form of scatter plot and error histogram (one after another). Herein, the performances of the tested models are reported for the training dataset only.

In addition, to assess the performance of the proposed models in another way, visual interpretations of results are presented in the form of a Taylor diagram and Accuracy matrix. The data visualization presents raw data through graphical representations that allow viewers to explore the data and uncover deep insights with ease, while enabling researchers to make a quick and compelling comparison of the models. The Taylor diagram [86] is a two-dimensional mathematical diagram designed for comparative assessment of multiple models in a single diagram in terms of the coefficient of correlation, RMSE, and ratio of their standard deviations. It is used to quantify the degree of correspondence between the actual and predictive models. Inside the diagram, each model is represented either by marking a ‘point’ or a ‘character’, whereby the marked point closer to the reference (Ref) point indicates a more accurate model. On the other hand, the Accuracy matrix is a novel heat map matrix introduced in this study, in which the values of performance indices are shown in terms of accuracies achieved w.r.t. their ideal values. For example, the ideal values of RMSE and R^2 are 0 and 1, respectively. In the present work, the values of these indices

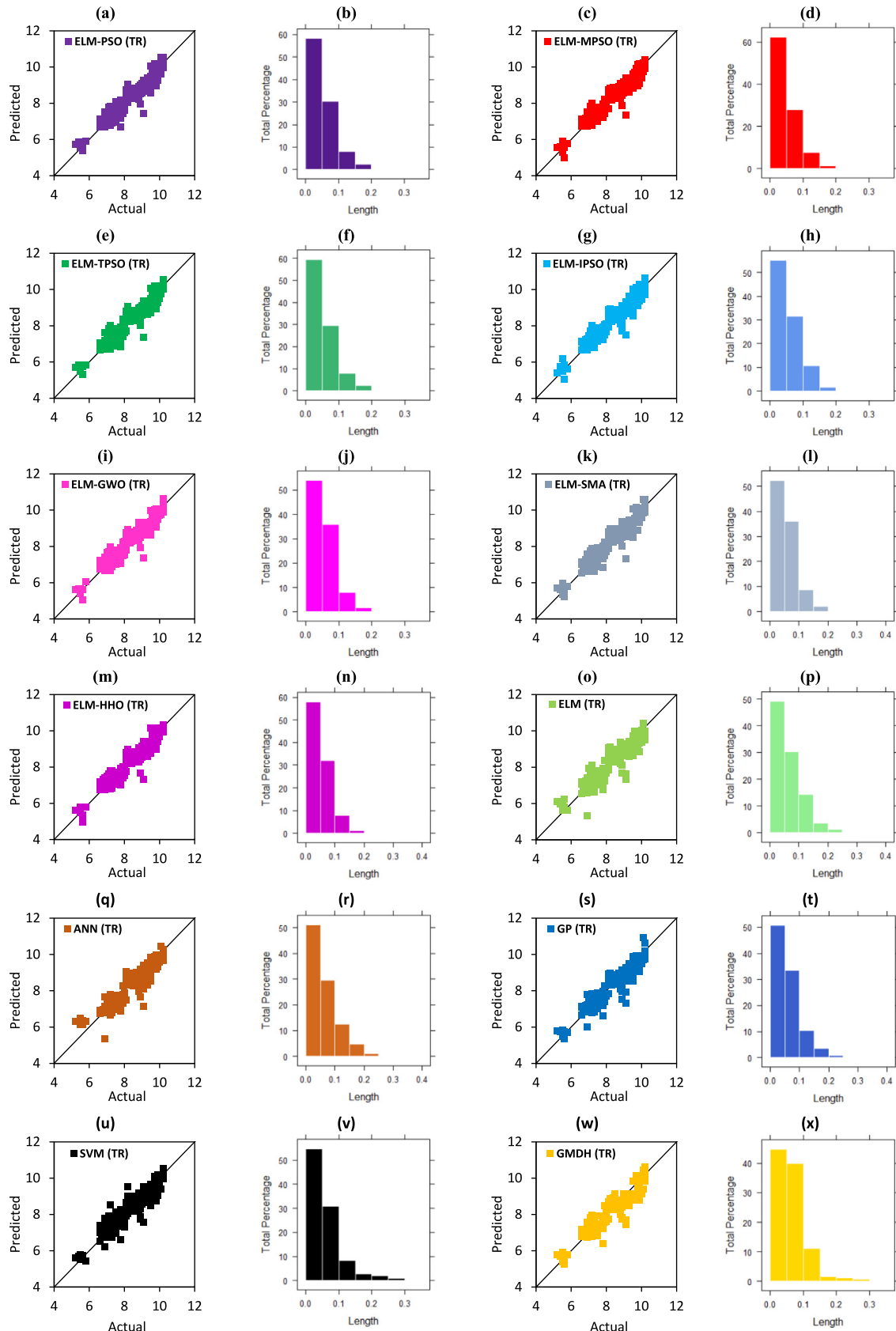


Fig. 7. Illustration of actual vs predicted values in the form of scatter plot and error histogram, respectively for: (a-b) ELM-PSO; (c-d) ELM-MPSO; (e-f) ELM-TPSO; (g-h) ELM-IPSO; (i-j) ELM-GWO; (k-l) ELM-SMA; (m-n) ELM-HHO; (o-p) ELM; (q-r) ANN; (s-t) GP; (u-v) SVM; and (w-x) GMDH models for the training dataset.

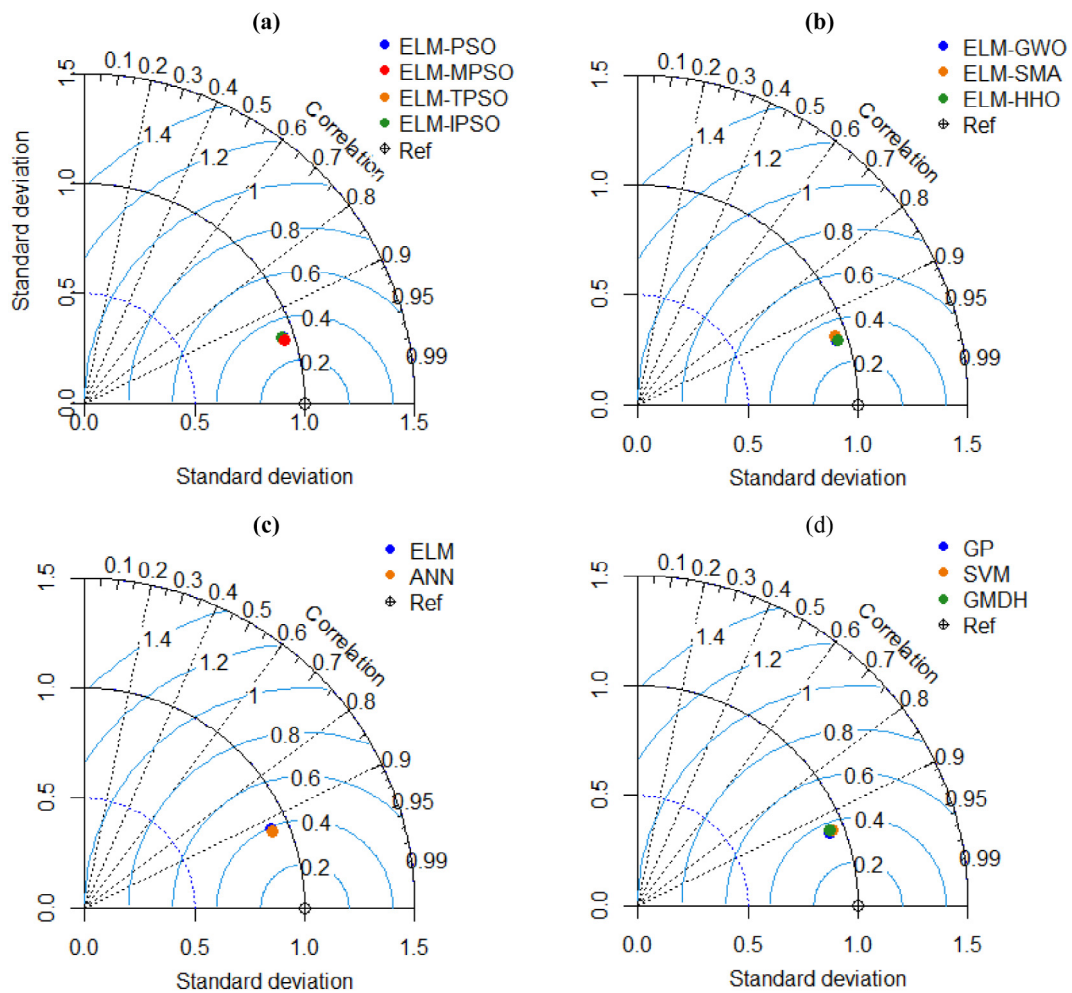


Fig. 8. (a–c) Taylor diagrams for the training dataset.

	ELM-PSO	ELM-MPSO	ELM-TPSO	ELM-IPSO	ELM-GWO	ELM-SMA	ELM-HHO	ELM	ANN	GP	SVM	GMDH	
R ²	90%	91%	90%	90%	90%	89%	91%	85%	86%	87%	87%	87%	100%
VAF	90%	91%	90%	90%	90%	89%	91%	85%	86%	87%	87%	87%	
PI	86%	88%	87%	86%	87%	86%	87%	80%	81%	83%	83%	82%	
WI	97%	98%	97%	97%	97%	97%	98%	96%	96%	97%	97%	96%	92%
MAE	95%	95%	95%	95%	95%	94%	95%	94%	94%	94%	94%	94%	
MAPE	89%	89%	89%	89%	89%	89%	89%	86%	83%	88%	88%	88%	
MBE	100%	100%	100%	100%	100%	100%	100%	100%	100%	100%	100%	100%	
RMSE	93%	94%	93%	93%	93%	93%	93%	92%	92%	92%	92%	92%	80%

Fig. 9. Accuracy matrix for the training results.

were calculated as 0.0645 and 0.9100, respectively, for the ELM-MPSO model (refer to **Table 5**). Therefore, it can be interpreted that the model achieved 93.55% ($1-0.0645 = 0.9355$) and 91.00% ($0.9100/1=0.9100$) accuracy in terms of RMSE and R^2 , respectively. Similarly, the values of PI and MAE were obtained as 1.7255 and 0.0530, respectively, for the ELM-PSO model, which indicates that the model achieved 86.275% ($1.7255/2=0.86275$) and 94.70% ($1-0.0530 = 0.9470$) accuracy in terms of PI and MAE , respectively. The same procedure was followed for the other indices as well.

Fig. 8(a–c) display the Taylor diagrams, indicating the relative accuracy of the developed models for the training dataset. Note that a model can be reported as ideal when the 'point' position is closer to the 'Ref' point (marked with a black circle). From **Fig. 8(a–d)**, it can be interpreted that the ELM-MPSO model attained the highest predictive accuracy as the model is closer to the 'Ref' point. In contrast, the Accuracy matrix for the developed models presented in **Fig. 9** reveals that the ELM-MPSO model attained the highest predictive accuracy in all stages (green colour indicates higher accuracy). One can easily refer to the heat map matrix to identify the degree of accuracy achieved in each case.

5.4. Validation of the proposed models

It is pertinent to mention that a model with higher predictive accuracy attained in the validation phase indicates a more accurate and robust model. Moreover, a higher predictive accuracy achieved in the training phase does not necessarily mean a better predictive model, and hence, proper validation of the model should be ensured. Therefore, it is practical to check the accuracy of any predictive model for the new dataset, since a predictive model validated with additional datasets obtained from different experiments (performed in different conditions/environments/set-ups) can be considered practically significant. In the present study, three-level validations were adopted: (1) the unused dataset, i.e., the testing dataset, extracted from the main dataset (validation level 1); (2) the experimental database (validation level 2) obtained from laboratory experiments (separate experiments were performed in geotechnical engineering laboratory); and (3) the simulated dataset (validation level 3). The predictive performance of the developed models for the new dataset was determined according to the three validation levels and is presented in the following sub-sections.

(a) 1st Level Validation (Level-1 Validation)

The 1st level validation was performed for the unused dataset, i.e., testing dataset (a portion of the main dataset based on 5-fold cross-validation), and the prediction outcomes of all the proposed models are furnished in **Table 6**. As can be seen, the ELM-MPSO model attained the most accurate prediction with $R^2 = 0.9248$, $PI = 1.7765$, $MAE = 0.0435$, and $RMSE = 0.0616$. ELM-TPSO and ELM-HHO were found to be the second and third-best predictive models, respectively. A detailed review of the results reveals that the ANN model attained the lowest predictive accuracy and found worst performing model compared to the accuracy attained in the training phase. On the other hand, the ELM-MPSO model attained the highest predictive accuracy in both phases, which indicates its robustness. Based on the experimental results, the proposed ELM-MPSO model attained the best performance in the level-1 validation phase. The predictive results of all models are illustrated in **Fig. 10(a–x)** in the form of scatter plots and error histograms (figures are placed in order). The Taylor diagrams and Accuracy matrix for the testing results are presented in **Fig. 11(a–d)** and **Fig. 12**, respectively. Herein, the performance of the developed models is reported for the testing dataset only. In

Figs. 10–12, the degree of correlation and the accuracies attained by the models can quickly be established.

(b) 2nd Level Validation (Level-2 Validation)

Furthermore, to assess the generalization capability of the proposed models, 2nd level validation was performed. For this purpose, separate laboratory experiments were conducted at the geotechnical laboratory of National Institute of Technology Patna, and 40 new datasets were generated. **Table 7** presents the descriptive statistics of the experimental datasets. As can be seen, most of the soils have gravel (G) and the sand contents (S) between 0%–10% and 22%–76%, respectively, while the content of silt and clay (S&C) lies in the range of 24%–73%. The MDD and OMC vary between 1.81–2.03 gm/cm³ and 7.50–15.50%, respectively. The values of soaked CBR are in the range of 6.30–10.12%. **Fig. 13** shows the experimental set-up used in this study to perform the laboratory experiments for: (a) grain size analysis; (b) analysis of PI; (c) determination of OMC and MDD; and d) determination of CBR. **Fig. 14** represents stacked histograms of each soil parameter, which are very useful, as they can help identify the range of parameter values present in the dataset.

Table 8 presents the prediction performance of the first nine best-performing models. It may be noted that, for a fair comparison, the performance of the ANN, GP, and GMDH models are not considered for further analysis due to the fact that their performance was unsatisfactory in the level-1 validation phase. However, the presented results show that the ELM-MPSO model outperformed the other models by far with $R^2 = 0.9885$ and $RMSE = 0.0164$, followed by ELM-TPSO, ELM-GWO, ELM-HHO, ELM-PSO, ELM-SMA, ELM-IPSO, SVM, and ELM (refer to **Table 8**). As can be seen, again, the ELM-TPSO model was found to be the second-best model in this phase, while the classical ELM exhibited the worst performance. The predictive results of the models are shown in **Fig. 15(a–i)** in the form of scatter plots, line plots, and error histograms (figures are placed in order), from which the goodness of fit of the proposed models, especially the performance of the ELM-MPSO model, can be visualized.

In addition, the values of A_{10} were calculated separately for the training dataset, 1st level validation dataset, and 2nd level validation dataset and are presented in **Table 9**. It can be observed that the ELM-based models achieved higher accuracy in all phases. Thus, it can be inferred in line with the methodology presented in Section 4.2 that, the ratio of experimental and predicted values of 100% data lies between 0.90 and 1.10. Both ELM-MPSO and ELM-GWO attained 98.40%, 98.39%, and 100% accuracy, respectively for the training, level-1, and level-2 databases, and were found to be best-performing models followed by other ELM-based models, SVM, and ELM (refer to **Table 9**).

5.5. Uncertainty analysis (UA) and statistical testing

The assessment of the trustworthiness of any predictive model is essential for the reliable and accurate estimation of predictive outputs. In the present study, uncertainty analysis (UA) has been performed to describe the quantitative assessment of error of the proposed models in predicting the CBR of soils in soaked conditions. The UA was performed for the training, level-1, and level-2 datasets, which respectively include 250, 62, and 40 experimental data of different soils. Hence, the comparison of predictive outputs with these experimental datasets is significant in assessing the reliability of the developed models, and UA is ideally suitable for this purpose. To perform UA, the absolute error (ε_i) between the actual (y_i) and predicted (\tilde{y}_i) value was calculated using the expression $\varepsilon_i = |(y_i - \tilde{y}_i)|$. Successively, the mean of error (MOE) of prediction and standard deviation

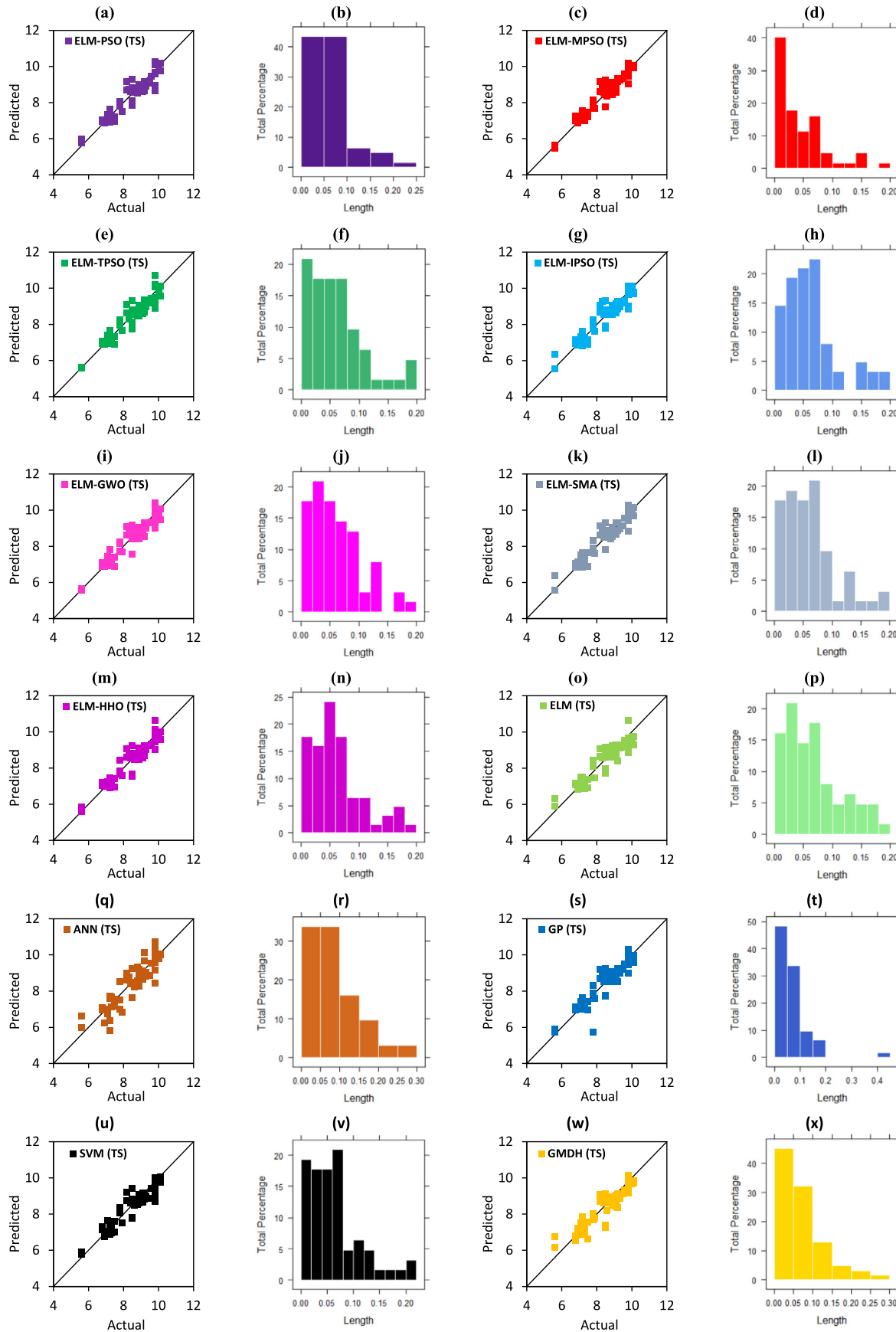


Fig. 10. Illustration of actual vs predicted values in the form of scatter plot and error histogram, respectively for: (a-b) ELM-PSO; (c-d) ELM-MPSO; (e-f) ELM-TPSO; (g-h) ELM-IPSO; (i-j) ELM-GWO; (k-l) ELM-SMA; (m-n) ELM-HHO; (o-p) ELM; (q-r) ANN; (s-t) GP; (u-v) SVM; and (w-x) GMDH models for the level-1 validation dataset.

Table 6
Details of performance indices for the testing dataset (level-1 validation).

Models	Performance indices							
	R ²	VAF	PI	WI	MAE	MAPE	MBE	RMSE
ELM-PSO	0.8904	89.0381	1.6890	0.9697	0.0598	11.5201	-0.0116	0.0752
ELM-MPSO	0.9248	92.4697	1.7765	0.9803	0.0435	7.9912	0.0000	0.0616
ELM-TPSO	0.8917	89.1301	1.6917	0.9704	0.0596	9.6044	-0.0119	0.0749
ELM-IPSO	0.8813	88.1276	1.6669	0.9673	0.0626	13.2519	-0.0081	0.0778
ELM-GWO	0.8904	89.0410	1.6895	0.9701	0.0609	10.2523	-0.0088	0.0748
ELM-SMA	0.8871	88.6888	1.6814	0.9688	0.0609	12.8582	-0.0020	0.0755
ELM-HHO	0.8906	89.0490	1.6896	0.9701	0.0600	10.5957	-0.0101	0.0750
ELM	0.8681	86.6166	1.6319	0.9609	0.0673	14.1832	-0.0085	0.0825
ANN	0.8008	77.5627	1.4390	0.9431	0.0855	19.2389	-0.0150	0.1074
GP	0.8467	84.4470	1.5783	0.9573	0.0647	12.2515	-0.0143	0.0897
SVM	0.8739	87.3288	1.6475	0.9637	0.0647	12.3818	-0.0108	0.0806
GMDH	0.8396	83.9513	1.5640	0.9533	0.0696	17.4656	-0.0134	0.0909

Table 7
Descriptive statistics of 40 new experimental datasets.

Statistical param.	G	S	S&C	PI	MDD	OMC	CBR
Minimum	0.00	22.00	24.00	0.00	1.81	7.50	6.30
Median	0.00	56.00	43.00	0.00	1.91	9.15	8.74
Mean	1.63	55.28	43.10	4.88	1.91	9.25	8.59
Maximum	10.00	76.00	73.00	21.00	2.03	15.50	10.12
Standard error	0.36	2.03	1.93	1.21	0.01	0.31	0.12
Standard deviation	2.27	12.84	12.21	7.67	0.04	1.95	0.75
Variance	5.16	164.92	149.12	58.78	0.00	3.78	0.56
Skewness	1.78	-0.85	0.72	1.02	0.35	1.96	-0.95
Kurtosis	3.76	0.58	0.17	-0.82	3.41	3.95	2.60
No. of dataset	40	40	40	40	40	40	40

Table 8
Details of performance indices for the experimental dataset (level-2 validation).

Models	Performance indices							
	R ²	VAF	PI	WI	MAE	MAPE	MBE	RMSE
ELM-PSO	0.9559	94.72	1.8555	0.9859	0.0275	5.4411	0.0125	0.0362
ELM-MPSO	0.9885	98.82	1.9574	0.9970	0.0116	1.7638	-0.0034	0.0164
ELM-TPSO	0.9619	94.00	1.8557	0.9866	0.0256	5.1520	0.0020	0.0363
ELM-IPSO	0.9507	92.25	1.8136	0.9781	0.0304	6.0473	-0.0223	0.0468
ELM-GWO	0.9580	94.96	1.8594	0.9850	0.0299	5.3664	-0.0173	0.0374
ELM-SMA	0.9539	94.42	1.8507	0.9866	0.0268	4.3653	0.0056	0.0354
ELM-HHO	0.9570	95.36	1.8667	0.9881	0.0232	4.0001	-0.0075	0.0327
ELM	0.8574	76.10	1.5086	0.9498	0.0510	9.9336	0.0090	0.0729
SVM	0.9211	87.26	1.7202	0.9723	0.0303	5.9853	-0.0064	0.0532

Table 9
Values of accuracy index (for training, level-1, and level-2 databases).

Database	ELM-PSO	ELM-MPSO	ELM-TPSO	ELM-IPSO	ELM-GWO	ELM-SMA	ELM-HHO	ELM	SVM
Training	98.00	98.40	98.40	97.20	98.40	97.60	98.40	94.40	94.80
Level-1	96.77	98.39	95.16	95.16	98.39	95.16	96.77	96.77	96.77
Level-2	97.50	100.00	100.00	97.50	100.00	97.50	100.00	95.00	97.50

(SD) were calculated. Furthermore, the margin of error (ME) was calculated at the 95% confidence level (i.e., $\alpha = 0.05$) to obtain the width of confidence bound (WCB). The 95% prediction error intervals represent an error range in which approximately 95% of the data is located. Standard error (SE), upper bound (UB) and lower bound (LB) were then calculated for the predicted values of each model. For any good model, the difference between the lower bound and upper bound values of the error, i.e. the WCB value, should be as small as possible [87]. The results of the UA are furnished in Table 10 along with a bar plot in Fig. 16(a-c).

Note that only the first nine best performing models (ELM-MPSO, ELM-TPSO, ELM-IPSO, ELM-PSO, ELM-GWO, ELM-SMA, ELM-HHO, ELM, and SVM) found in the level-1 validation phase were considered in UA. It is understood from the results that the

ELM-MPSO model achieved the lowest WCB values of 0.0102, 0.0222, and 0.0146, respectively for the training, level-1, and level-2 datasets compared to the other ELM-based models, and thus is the most accurate in predicting the CBR of soils. Moreover, the highest WCB values of the ELM and SVM models indicate greater uncertainty. Based on the WCB value, the models were ranked, from which the superiority of the ELM-MPSO (secured 1st rank in all cases) over other ELM-based models can be established. The values of WCB for the different datasets are presented in Fig. 16(a-c) in the form of a bar plot.

In addition to the UA, one-tailed statistical test (t-test) was performed to test the significant difference of the ELM-MPSO's performance against the other models in estimating the CBR of soil in soaked conditions. The one tailed t-test was performed on

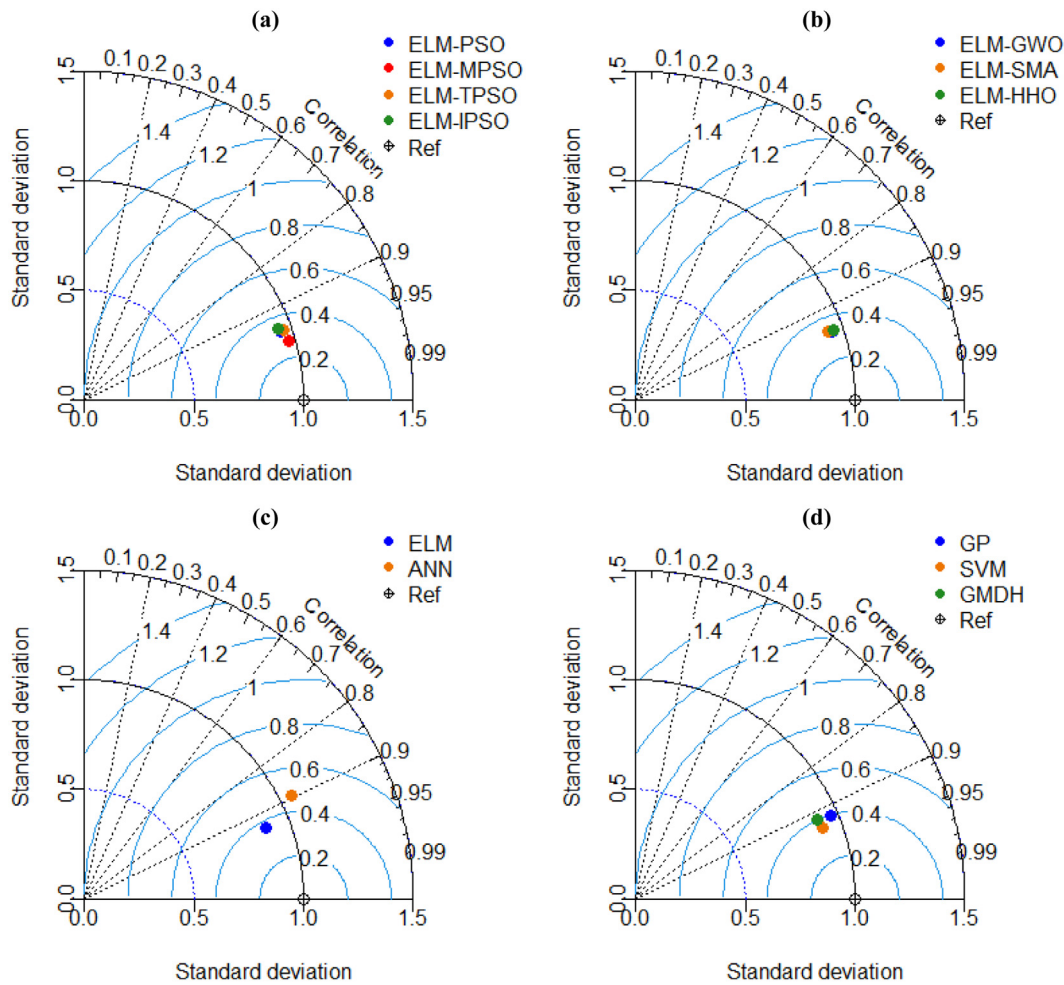


Fig. 11. (a–c) Taylor diagrams for the testing dataset (level-1 validation).

	ELM-PSO	ELM-MPSO	ELM-TPSO	ELM-IPSO	ELM-GWO	ELM-SMA	ELM-HHO	ELM	ANN	GP	SVM	GMDH	
R ²	89%	92%	89%	88%	89%	89%	89%	87%	80%	85%	87%	84%	100%
VAF	89%	92%	89%	88%	89%	89%	89%	87%	78%	84%	87%	84%	
PI	84%	89%	85%	83%	84%	84%	84%	82%	72%	79%	82%	78%	
WI	97%	98%	97%	97%	97%	97%	97%	96%	94%	96%	96%	95%	91%
MAE	94%	96%	94%	94%	94%	94%	94%	93%	91%	94%	94%	93%	
MAPE	88%	92%	90%	87%	90%	87%	89%	86%	81%	88%	88%	83%	
MBE	99%	100%	99%	99%	99%	100%	99%	99%	98%	99%	99%	99%	
RMSE	92%	94%	93%	92%	93%	92%	93%	92%	89%	91%	92%	91%	72%

Fig. 12. Accuracy matrix for the testing dataset (level-1 validation).

the MAE values considering that the hypothesized mean difference is equal to zero. The hypotheses for implementing the t-test

are: Null hypothesis - H_0 : $MAE_{ELM-MPSO} - MAE_{othermodels} = 0$; Alternate hypothesis - H_A : $MAE_{ELM-MPSO} - MAE_{other-models} < 0$;

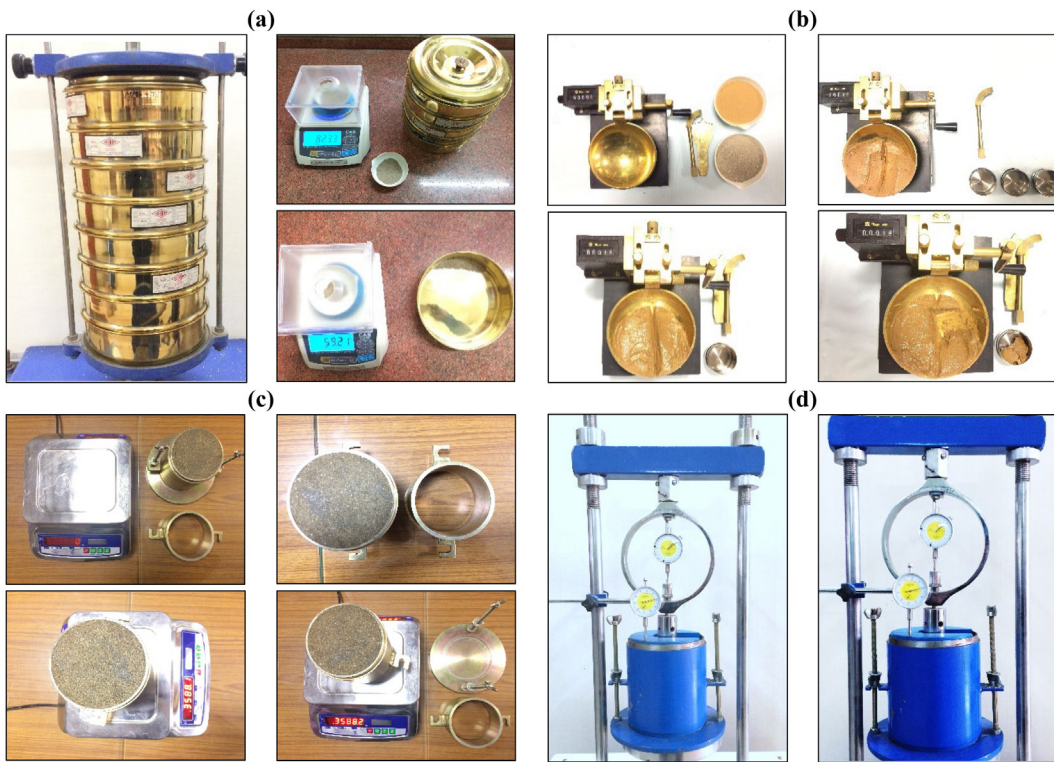


Fig. 13. Experimental setup for testing the soaked CBR along with other basic soil properties: (a) Sieve analysis, (b) Plastic limit test, (c) OMC and MDD test, and (d) CBR test.

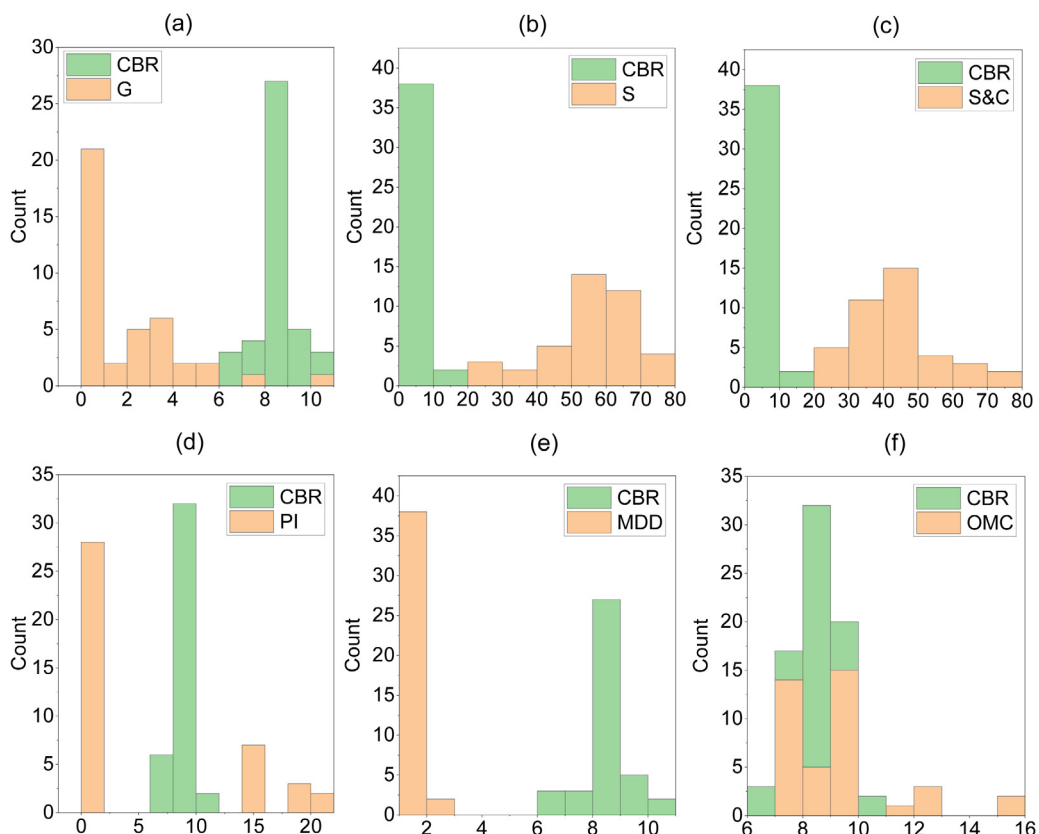


Fig. 14. Comparative histograms of the soil parameters and CBE for 40 new experimental datasets.

Table 10
Results of uncertainty analysis.

Levels	Models	MOE	SD	SE	ME	LB	UB	WCB	Rank
Training dataset	ELM-PSO	0.0530	0.0433	0.0027	0.0054	0.0476	0.0584	0.0108	5
	ELM-MPSO	0.0498	0.0410	0.0026	0.0051	0.0447	0.0549	0.0102	1
	ELM-TPSO	0.0509	0.0435	0.0028	0.0054	0.0455	0.0563	0.0108	6
	ELM-IPSO	0.0538	0.0423	0.0027	0.0053	0.0485	0.0591	0.0106	4
	ELM-GWO	0.0533	0.0416	0.0026	0.0052	0.0481	0.0585	0.0104	3
	ELM-SMA	0.0550	0.0438	0.0028	0.0055	0.0495	0.0605	0.0110	7
	ELM-HHO	0.0508	0.0419	0.0026	0.0052	0.0456	0.0560	0.0104	2
	ELM	0.0643	0.0545	0.0034	0.0068	0.0575	0.0711	0.0136	9
Level-1 dataset	SVM	0.0580	0.0510	0.0032	0.0064	0.0516	0.0644	0.0128	8
	ELM-PSO	0.0598	0.0456	0.0058	0.0116	0.0482	0.0714	0.0232	6
	ELM-MPSO	0.0435	0.0436	0.0055	0.0111	0.0324	0.0546	0.0222	1
	ELM-TPSO	0.0596	0.0454	0.0058	0.0115	0.0481	0.0711	0.0230	4
	ELM-IPSO	0.0626	0.0461	0.0059	0.0117	0.0509	0.0743	0.0234	7
	ELM-GWO	0.0617	0.0453	0.0058	0.0115	0.0502	0.0732	0.0230	5
	ELM-SMA	0.0609	0.0446	0.0057	0.0113	0.0496	0.0722	0.0226	2
	ELM-HHO	0.0600	0.0449	0.0057	0.0114	0.0486	0.0714	0.0228	3
	ELM	0.0673	0.0478	0.0061	0.0121	0.0552	0.0794	0.0242	8
Level-2 dataset	SVM	0.0647	0.0481	0.0061	0.0122	0.0525	0.0769	0.0244	9
	ELM-PSO	0.0365	0.0318	0.0040	0.0081	0.0284	0.0446	0.0162	2
	ELM-MPSO	0.0211	0.0286	0.0036	0.0073	0.0138	0.0284	0.0146	1
	ELM-TPSO	0.0370	0.0353	0.0045	0.0090	0.0280	0.0460	0.0180	5
	ELM-IPSO	0.0383	0.0359	0.0046	0.0091	0.0292	0.0474	0.0182	6
	ELM-GWO	0.0431	0.0384	0.0049	0.0098	0.0333	0.0529	0.0196	7
	ELM-SMA	0.0372	0.0321	0.0041	0.0082	0.0290	0.0454	0.0164	4
	ELM-HHO	0.0332	0.0317	0.0040	0.0081	0.0251	0.0413	0.0162	3
	ELM	0.0561	0.0521	0.0066	0.0132	0.0429	0.0693	0.0264	9
	SVM	0.0460	0.0513	0.0065	0.0130	0.0330	0.0590	0.0260	8

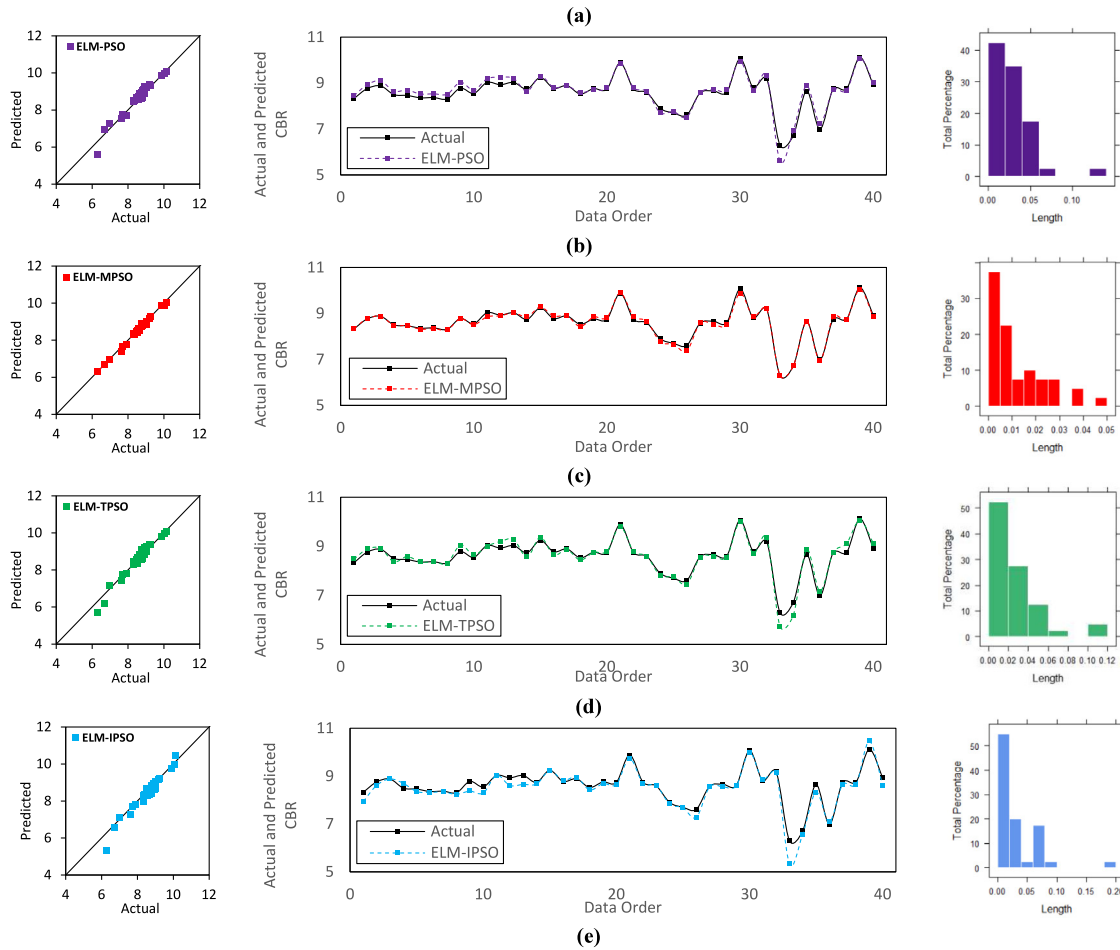


Fig. 15. (a-i) Illustration of actual vs predicted values, respectively for level-2 validation (in order: scatter plot, line plot, and error histogram) phase.

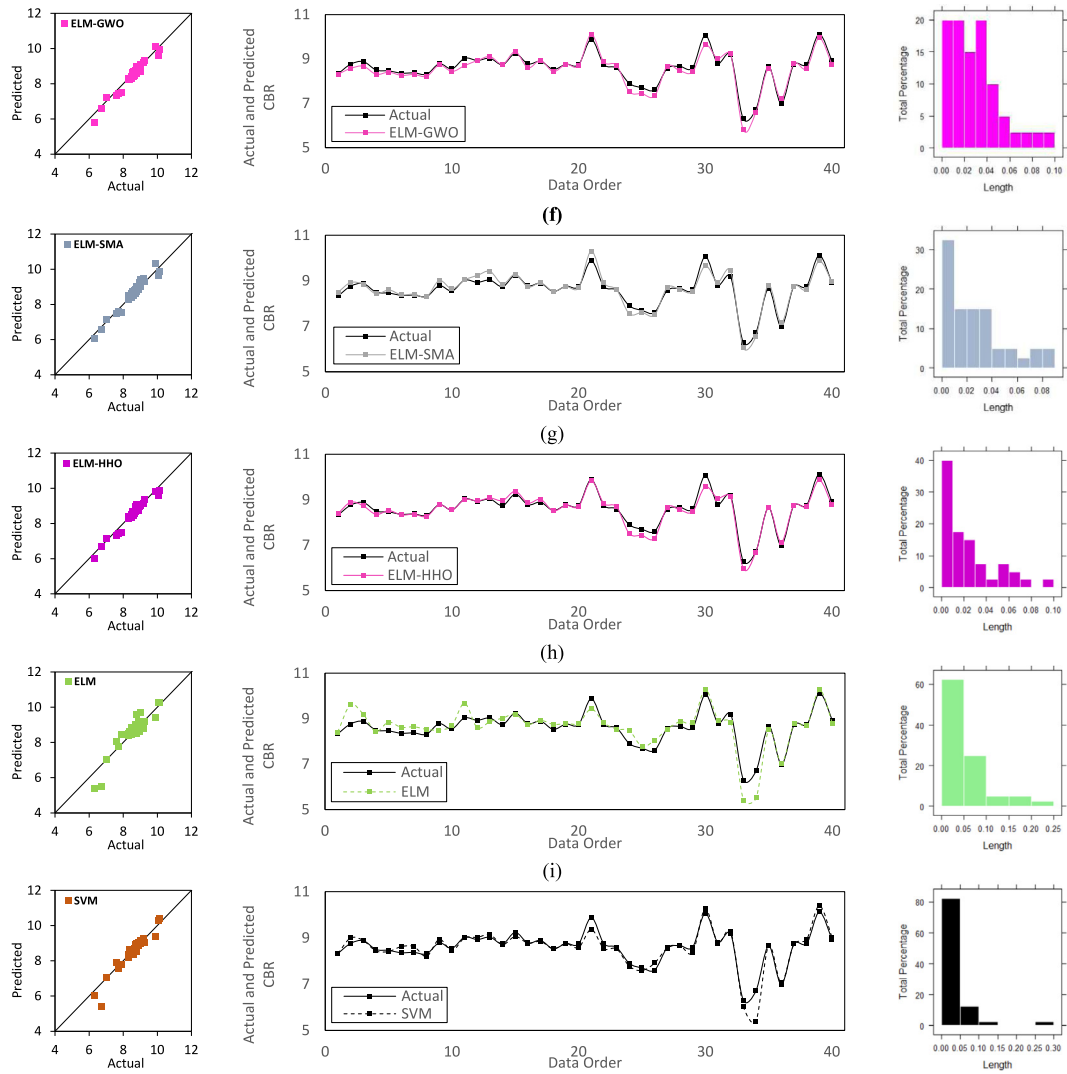


Fig. 15. (continued).

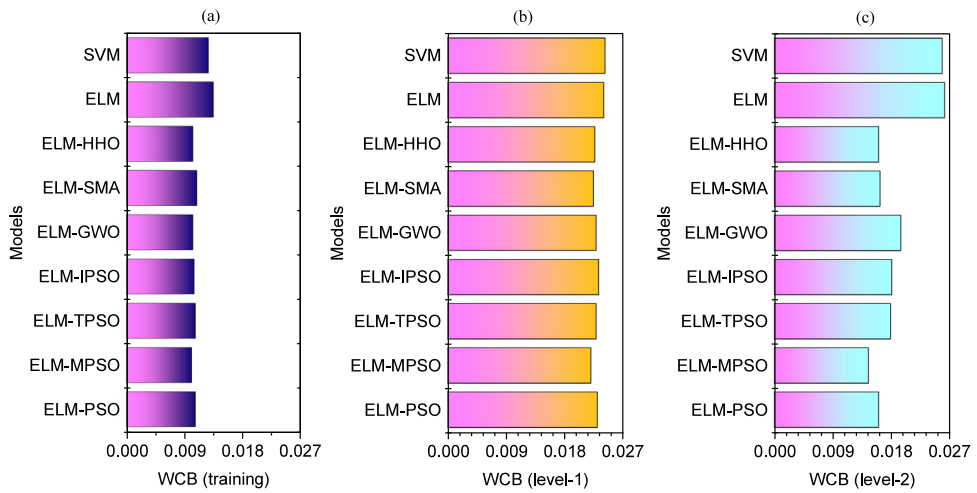


Fig. 16. Bar plot of WCB values for: (a) training dataset; (b) level-1 validation dataset; and (c) level-2 validation dataset.

$\alpha = 0.05$, and hypothesized mean difference (HMD) = 0. The obtained results are presented in Table 11. The rejection of H_0 in all cases ($t\text{-stat} < t\text{-critical}$) indicates that the ELM-MPSO model

significantly outperformed the other models in reducing the MAE value of the prediction model.

Table 11

Results of statistical test (one tailed t-test).

Level	Particulars	ELM-PSO	ELM-TPSO	ELM-IPSO	ELM-GWO	ELM-SMA	ELM-HHO	ELM	SVM
Training dataset	Samples	250	250	250	250	250	250	250	250
	HMD	0	0	0	0	0	0	0	0
	dof	249	249	249	249	249	249	249	249
	t-stat	-1.74	-0.83	-1.97	-1.72	-2.82	-0.67	-4.75	-3.21
	t-critical (one-tail)	1.65	1.65	1.65	1.65	1.65	1.65	1.65	1.65
	H_0	Reject	Reject	Reject	Reject	Reject	Reject	Reject	Reject
Level-1 dataset	Samples	62	62	62	62	62	62	62	62
	HMD	0	0	0	0	0	0	0	0
	dof	61	61	61	61	61	61	61	61
	t-stat	-2.86	-2.98	-3.60	-3.47	-3.34	-3.17	-3.67	-3.73
	t-critical (one-tail)	1.67	1.67	1.67	1.67	1.67	1.67	1.67	1.67
	H_0	Reject	Reject	Reject	Reject	Reject	Reject	Reject	Reject
Level-2 dataset	Samples	40	40	40	40	40	40	40	40
	HMD	0	0	0	0	0	0	0	0
	dof	39	39	39	39	39	39	39	39
	t-stat	-3.40	-2.78	-2.97	-5.33	-3.52	-3.38	-4.57	-2.50
	t-critical (one-tail)	1.68	1.68	1.68	1.68	1.68	1.68	1.68	1.68
	H_0	Reject	Reject	Reject	Reject	Reject	Reject	Reject	Reject

5.6. 3rd level validation (level-3 validation)

It is pertinent to mention that overfitting is a common problem usually encountered during the course of computational modelling [88]. This phenomenon directs that an AI model may predict the desired output in an excellent manner for a particular dataset in both training and testing phases. However, at the same time, it can predict exceptionally unusual results for other datasets obtained from a completely different experimental set-up. Hence, a predictive model should also be validated with other datasets. It is also worthy to assess the overall behaviour of a predictive model with regards to its expected behaviour for the simulated dataset. Although the proposed ELM-MPSO model performed significantly better in the level-2 validation phase, 3rd level validation was performed by employing simulated datasets to ensure the overall behaviour and the expected trend of the ELM-MPSO model. This obtained results provide a good indication that overfitting does not occur in the ELM-MPSO models.

One input parameter was changed to generate the simulated datasets, while the other input parameters were kept constant. For example, to ensure the trend between OMC and CBR, only the values of OMC were changed linearly, and the values of other parameters (G, S, S&C, PI, and MDD) were kept constant. For the MDD, the same procedure was followed. However, for the parameters G, S, and S&C, the basic principle of grain size distribution, i.e., the summation of the contents of G, S, and S&C cannot exceed 100%, was followed. Therefore, a linear increase in one parameter was adjusted by decreasing another parameter. In this study, four parameters, namely OMC, MDD, S, and S&C, were altered, and the simulated datasets were generated accordingly. The contents of S and S&C were altered.

Table 12 presents the details of the simulated datasets generated for four different cases (C1, C2, C3, and C4). The varying range of the input parameters in each case is also mentioned in Table 12. It may be noted that, to simulate the practical case, the summation of G, S, and S&C were kept exactly 100% in all cases. The OMC, MDD, S, S&C were selected near their minimum, maximum, and mean values. Also, to keep the proportion of G+S+S&C=100%, increase or decrease in S&C content, are adjusted with S content, and vice-versa.

Fig. 17 shows all the trends with smooth curves, as expected. In particular, Fig. 17(a-d) display the expected decrease in CBR with the increase in OMC, while Fig. 17(e-h) illustrate the reverse trend, i.e., increased CBR with an increase in MDD. On the other hand, the predicted CBR increased with the increase of sand (S) content (Fig. 17(i-l)), whereas the predicted CBR decreased

linearly as the silt and clay content (S&C) increase (Fig. 17 (m-p)). These simulated variations are consistent with the trend of the actual dataset, suggesting the correctness and robustness of the proposed ELM-MPSO model. As can be seen, the trends between CBR and OMC, MDD, S, and S&C obtained in the level-3 validation phase are in line with the trend of the actual dataset (refer to Fig. 5), verifying the robustness of the ELM-MPSO model. It is pertinent to note that the simulated datasets were used to ensure the expected trends of the simulated parameters through the ELM-MPSO model; however, real-life analysis may produce different results.

5.7. Discussion of results

In the above sub-sections, the developed AI-based models for predicting the CBR of soils in soaked conditions were assessed in detail. After the development of the models, 8 performance parameters (R^2 , VAF, PI, WI, MAE, MAPE, MBE and RMSE) were determined to evaluate the goodness of fit and the generalization capability of the prediction models. The obtained values of performance indices suggest that all the proposed models capture the relationship between soil parameters and CBR in the training stage; however, the ANN, GP, and GMDH models exhibit worse performance in the validation phase (level-1 validation phase). A comparison of the proposed models reveals that the ELM-MPSO model attained the highest predictive accuracy in both level-1 and level-2 validation phases, and outperformed the other ELM-based hybrid models by far. These results confirm the higher generalization capability and robustness of the ELM-MPSO model. The convergence performance further indicates that MPSO achieved a superior solution faster than the TPSO, IPSO, PSO, GWO, SMA, and HHO, confirming the superiority of the MPSO algorithm in ELM-based modelling. Based on the quantitative assessment of error (as per WCB value presented in Table 10), the ELM-MPSO model exhibits the highest degree of certainty compared to ELM-TPSO, ELM-IPSO, ELM-PSO, ELM-GWO, ELM-SMA, ELM-HHO, and other CSC models.

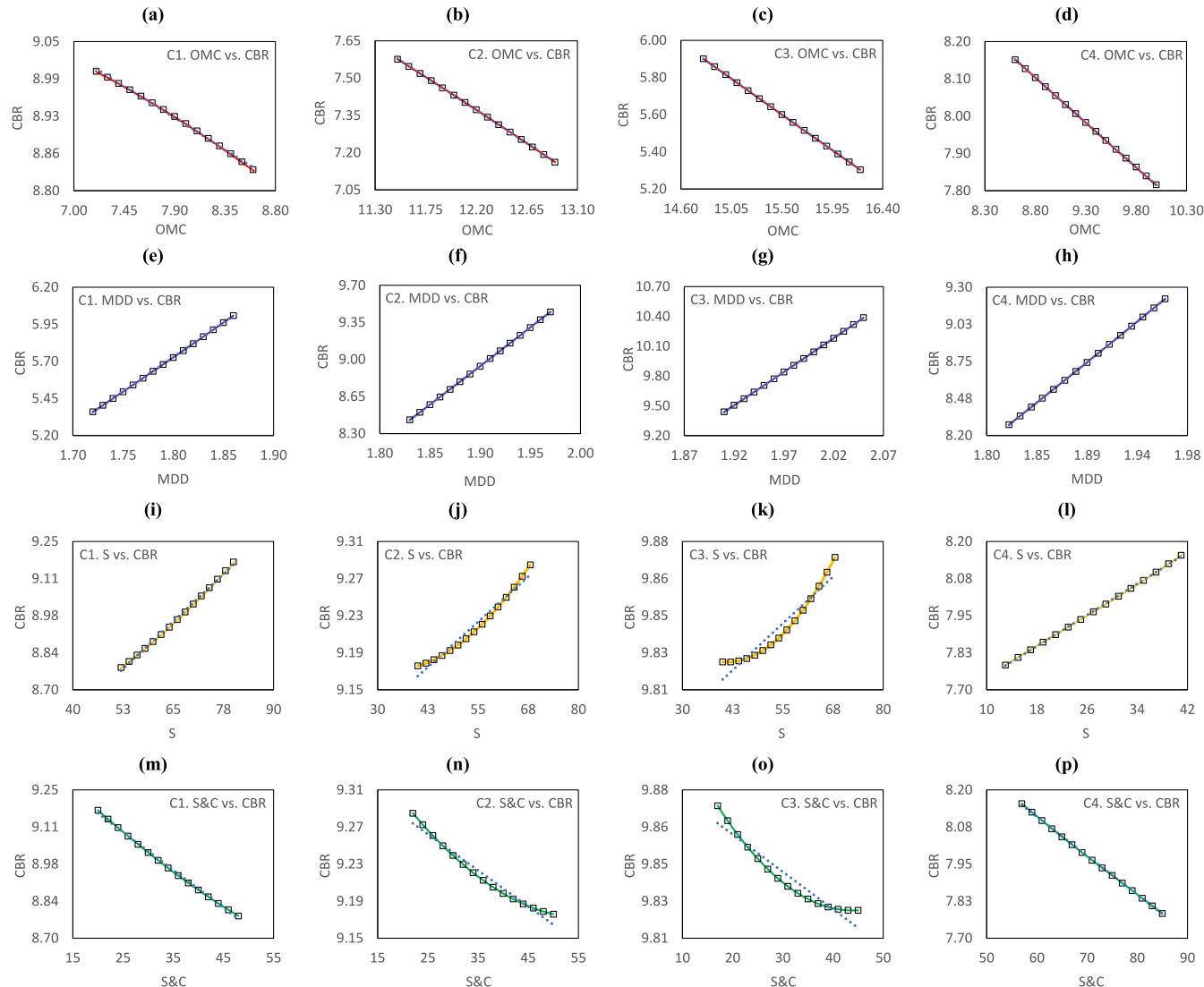
Furthermore, to compare the performance of the models graphically, a visual interpretation of results is presented in the form of a Taylor diagram and Accuracy matrix. The Taylor diagrams show a two-dimensional graphical plot for comparative assessment of the models in terms of correlation coefficient, RMSE, and ratio of standard deviation between the actual and predictive model, while the Accuracy matrix shows the degree of accuracy achieved against each performance index. Note that these diagrams are rather convenient for the quick assessment of results

Table 12

Details of simulated datasets.

Variable input parameter		No. of dataset	Constant input parameters	Fig. ref
Param.	Range			
OMC	C1: 7.20 – 8.60	15 × 4	C1: G = 4, S = 52, S&C = 44, PI = 0, MDD = 1.90	Fig. 17(a-d)
	C2: 11.50 – 12.90		C2: G = 0, S = 44, S&C = 56, PI = 13, MDD = 1.85.	
	C3: 14.80 – 16.20		C3: G = 6, S = 17, S&C = 77, PI = 26, MDD = 1.82.	
	C4: 8.60 – 10.00		C4: G = 2, S = 45, S&C = 53, PI = 5, MDD = 1.85.	
MDD	C1: 1.72 – 1.86	15 × 4	C1: G = 0, S = 17, S&C = 83, PI = 22, OMC = 14.90	Fig. 17(e-h)
	C2: 1.83 – 1.97		C2: G = 4, S = 52, S&C = 44, PI = 13, OMC = 7.80.	
	C3: 1.91 – 2.05		C3: G = 12, S = 61, S&C = 27, PI = 0, OMC = 7.30.	
	C4: 1.82 – 1.96		C4: G = 2, S = 58, S&C = 40, PI = 5, OMC = 7.80.	
S	C1: 52.00 – 80.00	15 × 4	C1: G = 0, PI = 0, MDD = 1.92, OMC = 7.80	Fig. 17(i-l)
	C2: 40.00 – 68.00		C2: G = 10, PI = 0, MDD = 1.91, OMC = 7.50.	
	C3: 40.00 – 68.00		C3: G = 15, PI = 0, MDD = 1.96, OMC = 7.20.	
	C4: 13.00 – 41.00		C4: G = 2, PI = 5, MDD = 1.84, OMC = 9.20.	
S&C	C1: 20.00 – 48.00	15 × 4	C1: G = 0, PI = 0, MDD = 1.92, OMC = 7.80	Fig. 17(m-p)
	C2: 22.00 – 50.00		C2: G = 10, PI = 0, MDD = 1.91, OMC = 7.50	
	C3: 17.00 – 45.00		C3: G = 15, PI = 0, MDD = 1.96, OMC = 7.20.	
	C4: 57.00 – 85.00		C4: G = 2, PI = 5, MDD = 1.84, OMC = 9.20.	

Note: C1 = Case 1; C2 = Case 2; C3 = Case 3; and C4 = Case 4.

**Fig. 17.** Illustration of level-3 validation phase: (a-d) C1-C4: OMC vs. CBR; (e-h) C1-C4: MDD vs. CBR; (i-l) C1-C4: S vs. CBR; (m-p) C1-C4: S&C vs. CBR.

without seeing the value of each index. Overall, the incorporation of time-varying acceleration coefficients generates higher prediction accuracy, which in turn satisfies the generalization capability and robustness of MPSO over SPSO in ELM-based ANSI models for predicting the CBR of soils.

6. Summary and conclusion

In many civil engineering projects, CBR is an essential parameter for determining the thickness of subgrade layers. Generally, laboratory tests are performed on the compacted soil samples in soaked conditions and require 4 days to complete, which is both time-consuming and expensive. Therefore, this study was motivated to replace the tedious operation of conducting actual laboratory tests with efficient machine-learning models for predicting CBR based on the existing experimental database. It is pertinent to mention that the accurate and reliable estimation of soaked CBR can save time and costs of conducting actual laboratory tests. For this purpose, experimental CBR values of fine-grained soils belonging to CL, CI, SC, ML, and SM groups were collected from an ongoing Indian Railways project and were used to develop an efficient machine-learning solution. The proposed approach is a novel integration of the ELM and ANSI techniques. In ELM-based ANSI modelling, PSO with adaptive and time-varying acceleration coefficients was used to optimize the learning parameters of ELM. To develop the prediction models of CBR, a total of 250 experimental results was used. Also, to validate the proposed models, three-level validations were adopted. Experimental outcomes show that the proposed ELM-MPSO model attained the most accurate prediction with $R^2 = 0.9248$, $PI = 1.7765$, $MAE = 0.0435$, and $RMSE = 0.0616$ in the level-1 validation phase, and with $R^2 = 0.9885$, $PI = 1.9574$, $MAE = 0.0116$, and $RMSE = 0.0164$ in the level-2 validation phase. Also, the results of the ELM-MPSO model are significantly better than those obtained by other ELM-based models, including the ELM-GWO, ELM-SMA, ELM-HHO, classical ELM and ANN, GP, SVM and GMDH. Considering the experimental results, the proposed ELM-MPSO model provides a new alternative to estimate the CBR of soaked soils using only the basic soil properties.

The present study aimed to substitute the tiresome process of conducting laboratory tests of CBR in soaked conditions and to expand upon earlier AI-based studies, indicating their outcomes of the developed models. Considering the gaps and limited findings of previous works, a widely used meta-heuristic OA, i.e., PSO, with adaptive and time-varying acceleration coefficients was used to expand the global search space of SPSO through ELM-based ANSI models (ELM-MPSO, ELM-TPSO, and ELM-IPSO). The experimental results show that the proposed ELM-MPSO model yielded the most desired prediction performance in terms of performance indices and convergence speed. The results also confirm the superiority of the ELM-MPSO model over the other ELM-based models, including the ELM-GWO, ELM-SMA, and ELM-HHO. Moreover, the prediction accuracy and accelerated convergence rate further verify that the implementation of time-varying acceleration coefficients offers a promising solution to handle the global search operation of the PSO algorithm.

The main advantages of the proposed ELM-MPSO model compared to classical ELM-PSO includes faster convergence rate and high accuracy. Based on the analyses presented above, the issues in selecting the deterministic values of acceleration coefficients of SPSO through trial-and-error approaches can be addressed by utilizing the proposed approaches. In addition, the results of the 40 new experimental datasets show that the proposed ELM-MPSO model attained a significant accuracy level and hence, can be used for predicting the soil CBR in soaked conditions. This is one of the major findings of this study and hence more researches on large

projects/laboratory experiments should be carried out to extend the application of the proposed model. However, the future direction of this study may include a more comprehensive assessment of the accuracy of MPSO, TPSO, IPSO, and PSO using real-time data from different fields; incorporation of adaptive and time-varying exploration and exploitation coefficients to expand the global search of other meta-heuristic algorithms along with a detailed comparison; assessment of superiority of the proposed ELM-based models over the ANN-based ANSI models (i.e., ANN-MPSO, ANN-TPSO, and ANN-IPSO); analyses of other ELM models with parallel layer perceptrons; a detailed comparison of ELM-based evolutionary optimization models for new datasets; and real-time validation of simulated results (analysed in this study) through laboratory experiments. To evaluate the practical application of the developed model in detail, the proposed approach can be adopted for predicting the CBR of soil in different engineering projects.

CRediT authorship contribution statement

Abidhan Bardhan: Conceptualization, Development of computational model, Detailing, Overall analysis, Manuscript finalization. **Pijush Samui:** Review of manuscript. **Kuntal Ghosh:** Detailed review and editing. **Amir H. Gandomi:** Detailed review and editing. **Siddhartha Bhattacharyya:** Detailed review and editing.

Declaration of competing interest

The authors declare that they have no known competing financial interests or personal relationships that could have appeared to influence the work reported in this paper.

Acknowledgements

The authors are very thankful to the Dedicated Freight Corridor of India Limited (DFCCIL) New Delhi, India and officials of L&T Construction, DFCCIL CTP-3(R) Project Site, Ahmedabad, India to provide experimental data and their kind support during this study.

References

- [1] D.J. Stephens, The prediction of the California bearing ratio, *Civ. Eng. Siviele Ingenieurswese*. 1990 (1990) 523–528.
- [2] B. Yildirim, O. Gunaydin, Estimation of California bearing ratio by using soft computing systems, *Expert Syst. Appl.* 38 (2011) 6381–6391, <https://doi.org/10.1016/j.eswa.2010.12.054>.
- [3] T. Taskiran, Prediction of California bearing ratio (CBR) of fine grained soils by AI methods, *Adv. Eng. Softw.* 41 (2010) 886–892, <https://doi.org/10.1016/j.advengsoft.2010.01.003>.
- [4] W. Black, A method of estimating the California bearing ratio of cohesive soils from plasticity data *, 1943, pp. 281–282.
- [5] D.G.-J. J.W.S., B. H.S., The engineering characteristics of the lateritic gravels of Ghana, in: Proceedings of 7th International Conference on Soil Mechanics and Foundation Engineering, vol. 2, Mexico, August 28–29, Asian Institute of Technology, Bangkok, 1969, pp. 13–43.
- [6] K.B. Agarwal, K.D. Ghanekar, Prediction of CBR from plasticity characteristics of soil, in: Proceeding 2nd South-East Asian Conf. Soil Eng., Singapore, 1970, pp. 11–15.
- [7] T. Al-Refeai, A. Al-Suhaimi, Prediction of CBR using dynamic cone penetrometer, *J. King Saud Univ. - Eng. Sci.* 9 (1997) 191–203, [https://doi.org/10.1016/S1018-3639\(18\)30676-7](https://doi.org/10.1016/S1018-3639(18)30676-7).
- [8] NCHRP, Guide for Mechanistic -Empirical Design of New and Rehabilitated Pavement Structures, NCHRP 1-37A Final Report, Appendix CC-4: Development of a Revised Predictive Model for the Dynamic (Complex) Modulus of Asphalt Mixtures, 2004, p. 8.
- [9] M.W. Kin, California Bearing Ratio Correlation with Soil Index Properties (Master Degree), Proj. Fac. Civ. Eng. Univ. Technol. Malaysia., 2006.

- [10] N. Puri, A. Jain, Correlation between California bearing ratio and index properties of silt and clay of low compressibility, in: Fifth Indian Young Geotech. Eng. Conf., 2015.
- [11] V.K. Varghese, S.S. Babu, R. Bijukumar, S. Cyrus, B.M. Abraham, Artificial neural networks: A solution to the ambiguity in prediction of engineering properties of fine-grained soils, *Geotech. Geol. Eng.* 31 (2013) 1187–1205.
- [12] S. Taha, A. Gabr, S. El-Badawy, Regression and neural network models for California bearing ratio prediction of typical granular materials in Egypt, *Arab. J. Sci. Eng.* 44 (2019) 8691–8705, <https://doi.org/10.1007/s13369-019-03803-z>.
- [13] G.V. Ramasubbarao, G. Siva Sankar, Predicting soaked CBR value of fine grained soils using index and compaction characteristics, *Jordan J. Civ. Eng.* 7 (2013) 354–360.
- [14] M.R. Islam, A.C. Roy, Prediction of California bearing ratio of fine-grained soil stabilized with admixtures using soft computing systems, *J. Civ. Eng. Sci. Technol.* 11 (2020) 28–44, <https://doi.org/10.3373/jcst.2035.2020>.
- [15] S. Bhatt, P.K. Jain, Prediction of california bearing ratio of soils using artificial neural network, *Am. Int. J. Res. Sci. Technol. Eng. Math.* (2014) 156–161.
- [16] R.S. Patel, M.D. Desai, CBR predicted by index properties for alluvial soils of South Gujarat, in: Indian Geotech. Conf., 2010, pp. 79–82, http://www.mddesai.com/Paper_2000_2010/20-020.pdf.
- [17] V.Y. Katte, S.M. Mfoyet, B. Manefouet, A.S.L. Wouatong, L.A. Bezeng, Correlation of California bearing ratio (CBR) value with soil properties of road subgrade soil, *Geotech. Geol. Eng.* 37 (2019) 217–234, <https://doi.org/10.1007/s10706-018-0604-x>.
- [18] S. Bhatt, P.K. Jain, Prediction of california bearing ratio of soils using artificial neural network, *Am. Int. J. Res. Sci. Technol. Eng. Math.* 8 (2014) 156–161.
- [19] S.K. Alam, A. Mondal, A. Shiuly, Prediction of CBR value of fine grained soils of bengal basin by genetic expression programming, artificial neural network and Krigging method, *J. Geol. Soc. India.* 95 (2020) 190–196.
- [20] S. Taha, A. Gabr, A. Azam, U. Shahdah, Modeling of california bearing ratio using basic engineering properties, 2014, pp. 1–9.
- [21] A. Ghorbani, H. Hasanzadehshoiloili, Prediction of UCS and CBR of microsilica-lime stabilized sulfate silty sand using ANN and EPR models; application to the deep soil mixing, *Soils Found.* 58 (2018) 34–49, <https://doi.org/10.1016/j.sandf.2017.11.002>.
- [22] Y. Erzin, D. Turkoz, Use of neural networks for the prediction of the CBR value of some Aegean sands, *Neural Comput. Appl.* 27 (2016) 1415–1426, <https://doi.org/10.1007/s00521-015-1943-7>.
- [23] A.R. Tenpe, A. Patel, Utilization of support vector models and gene expression programming for soil strength modeling, *Arab. J. Sci. Eng.* (2020) 1–19.
- [24] T. Fikret Kurnaz, Y. Kaya, Prediction of the California bearing ratio (CBR) of compacted soils by using GMDH-type neural network, *Eur. Phys. J. Plus* 134 (2019) 0–15, <https://doi.org/10.1140/epjp/i2019-12692-0>.
- [25] S. Al-Busultan, G.K. Aswed, R.R.A. Almuhamma, S.E. Rasheed, Application of artificial neural networks in predicting subbase CBR values using soil indices data, *IOP Conf. Ser. Mater. Sci. Eng.* 671 (2020) <https://doi.org/10.1088/1757-899X/671/1/012106>.
- [26] A.K. Sabat, Prediction of California bearing ratio of a stabilized expansive soil using artificial neural network and support vector machine, *Electron. J. Geotech. Eng.* 20 (2015) 981–991.
- [27] M. Suthar, P. Aggarwal, Predicting CBR value of stabilized pond ash with lime and lime sludge using ANN and MR models, *Int. J. Geosynth. Gr. Eng.* 4 (2018) <https://doi.org/10.1007/s40891-017-0125-3>.
- [28] I. González Farias, W. Araujo, G. Ruiz, Prediction of California bearing ratio from index properties of soils using parametric and non-parametric models, *Geotech. Geol. Eng.* 36 (2018) 3485–3498, <https://doi.org/10.1007/s10706-018-0548-1>.
- [29] S.K. Alam, A. Mondal, A. Shiuly, Prediction of CBR value of fine grained soils of Bengal basin by genetic expression programming, artificial neural network and Krigging method, *J. Geol. Soc. India.* 95 (2020) 190–196, <https://doi.org/10.1007/s12594-020-1409-0>.
- [30] A.K. Sabat, Prediction of california bearing ratio of a stabilized expansive soil using artificial neural network and support vector machine, *Electron. J. Geotech. Eng.* 20 (2015) 981–991.
- [31] H.L. Wang, Z.Y. Yin, High performance prediction of soil compaction parameters using multi expression programming, *Eng. Geol.* 276 (2020) 105758, <https://doi.org/10.1016/j.enggeo.2020.105758>.
- [32] M. Koopaliipoor, A. Fallah, D.J. Armaghani, A. Azizi, E.T. Mohamad, Three hybrid intelligent models in estimating flyrock distance resulting from blasting, *Eng. Comput.* 35 (2019) 243–256, <https://doi.org/10.1007/s00366-018-0596-4>.
- [33] S.-W. Liou, C.-M. Wang, Y.-F. Huang, Integrative discovery of multifaceted sequence patterns by frame-relayed search and hybrid PSO-ANN, *J. UCS* 15 (2009) 742–764.
- [34] L.T. Le, H. Nguyen, J. Dou, J. Zhou, A comparative study of PSO-ANN, GA-ANN, ICA-ANN, and ABC-ANN in estimating the heating load of buildings' energy efficiency for smart city planning, *Appl. Sci.* 9 (2019) <https://doi.org/10.3390/app9132630>.
- [35] H. Nikafshan Rad, I. Bakhsayeshi, W.A. Wan Jusoh, M.M. Tahir, L.K. Foong, Prediction of flyrock in mine blasting: A new computational intelligence approach, *Nat. Resour. Res.* 29 (2020) 609–623, <https://doi.org/10.1007/s11053-019-09464-x>.
- [36] M. Hasanipanah, D. Jahed Armaghani, H. Bakhsandeh Amniah, M.Z.A. Majid, M.M.D. Tahir, Application of PSO to develop a powerful equation for prediction of flyrock due to blasting, *Neural Comput. Appl.* 28 (2017) 1043–1050, <https://doi.org/10.1007/s00521-016-2434-1>.
- [37] D. Tien Bui, V.H. Nhu, N.D. Hoang, Prediction of soil compression coefficient for urban housing project using novel integration machine learning approach of swarm intelligence and Multi-layer Perceptron Neural Network, *Adv. Eng. Inf.* 38 (2018) 593–604, <https://doi.org/10.1016/j.aei.2018.09.005>.
- [38] H. Moayedi, A. Moatamediany, H. Nguyen, X.N. Bui, D.T. Bui, A.S.A. Rashid, Prediction of ultimate bearing capacity through various novel evolutionary and neural network models, *Eng. Comput.* 36 (2020) 671–687, <https://doi.org/10.1007/s00366-019-00723-2>.
- [39] B.R. Murlidhar, D. Kumar, D. Jahed Armaghani, E.T. Mohamad, B. Roy, B.T. Pham, A novel intelligent ELM-bbo technique for predicting distance of mine blasting-induced flyrock, *Nat. Resour. Res.* 29 (2020) 4103–4120, <https://doi.org/10.1007/s11053-020-09676-6>.
- [40] S.H. Min, J. Lee, I. Han, Hybrid genetic algorithms and support vector machines for bankruptcy prediction, *Expert Syst. Appl.* 31 (2006) 652–660, <https://doi.org/10.1016/j.eswa.2005.09.070>.
- [41] B. Roy, M.P. Singh, An empirical-based rainfall-runoff modelling using optimization technique, *Int. J. River Basin Manag.* 18 (2020) 49–67, <https://doi.org/10.1080/15715124.2019.1680557>.
- [42] L. Chen, L. Duan, Y. Shi, C. Du, PSO-LSSVM prediction model and its MATLAB implementation, *IOP Conf. Ser. Earth Environ. Sci.* 428 (2020) <https://doi.org/10.1088/1755-1315/428/1/012089>.
- [43] H.B. Ly, B.T. Pham, L.M. Le, T.T. Le, V.M. Le, P.G. Asteris, Estimation of axial load-carrying capacity of concrete-filled steel tubes using surrogate models, *Neural Comput. Appl.* (2020) 0123456789, <https://doi.org/10.1007/s00521-020-05214-w>.
- [44] D.J. Armaghani, M. Hajihassani, E.T. Mohamad, A. Marto, S.A. Noorani, Blasting-induced flyrock and ground vibration prediction through an expert artificial neural network based on particle swarm optimization, *Arab. J. Geosci.* 7 (2014) 5383–5396, <https://doi.org/10.1007/s12517-013-1174-0>.
- [45] M.N. Asmawisham Alel, M.R. Anak Upom, R.A. Abdullah, M.H. Zainal Abidin, Optimizing blasting's air overpressure prediction model using swarm intelligence, *J. Phys. Conf. Ser.* 995 (2018) <https://doi.org/10.1088/1742-6596/995/1/012046>.
- [46] M. Hasanipanah, A. Shahnaz, H. Bakhsandeh Amniah, D. Jahed Armaghani, Prediction of air-overpressure caused by mine blasting using a new hybrid PSO-SVR model, *Eng. Comput.* 33 (2017) 23–31, <https://doi.org/10.1007/s00366-016-0453-2>.
- [47] G. Bin Huang, Q.Y. Zhu, C.K. Siew, Extreme learning machine: Theory and applications, *Neurocomputing* 70 (2006) 489–501, <https://doi.org/10.1016/j.neucom.2005.12.126>.
- [48] Z. Cui, J. Zeng, Y. Yin, An improved PSO with time-varying accelerator coefficients, in: Proc. - 8th Int. Conf. Intell. Syst. Des. Appl. ISDA 2008, vol. 2, 2008, pp. 638–643, <https://doi.org/10.1109/ISDA.2008.86>.
- [49] F. Van Den Berg, A.P. Engelbrecht, A study of particle swarm optimization particle trajectories, *Inf. Sci. (Ny)* 176 (2006) 937–971, <https://doi.org/10.1016/j.ins.2005.02.003>.
- [50] G.Q. Bao, K.F. Mao, Particle swarm optimization algorithm with asymmetric time varying acceleration coefficients, in: 2009 IEEE Int. Conf. Robot. Biomimetics, ROBIO 2009, 2009, pp. 2134–2139, <https://doi.org/10.1109/ROBIO.2009.5420504>.
- [51] Y. Fukuyama, H. Yoshida, A particle swarm optimization for reactive power and voltage control in electric power systems, in: Proc. 2001 Congr. Evol. Comput. (IEEE Cat. No. 01TH8546), IEEE, 2001, pp. 87–93.
- [52] M. Hajihassani, D. Jahed Armaghani, H. Sohaili, E. Tonnizam Mohamad, A. Marto, Prediction of airblast-overpressure induced by blasting using a hybrid artificial neural network and particle swarm optimization, *Appl. Acoust.* 80 (2014) 57–67, <https://doi.org/10.1016/j.apacoust.2014.01.005>.
- [53] Z. Tang, D. Zhang, A modified particle swarm optimization with an adaptive acceleration coefficients, in: Proc. - 2009 Asia-Pacific Conf. Inf. Process. APCIP 2009., vol. 2, 2009, pp. 330–332. <http://dx.doi.org/10.1109/APCIP.2009.217>.
- [54] D. Serre, Iterative methods for linear problems, *Matrices Theory Appl.* (2002) 149–167.
- [55] C.R. Rao, S.K. Mitra, Further contributions to the theory of generalized inverse of matrices and its applications, *Sankhyā Indian J. Stat. Ser. A* (1971) 289–300.
- [56] C.R. Rao, S.K. Mitra, *Generalized Inverse of Matrices and its Applications*, John Wiley & Sons, Inc., New York, 1971).

- [57] M. Kumar, P. Samui, Reliability analysis of pile foundation using ELM and MARS, *Geotech. Geol. Eng.* 37 (2019) 3447–3457, <https://doi.org/10.1007/s10706-018-00777-x>.
- [58] N.D. Hoang, D. Tien Bui, Slope Stability Evaluation using Radial Basis Function Neural Network, Least Squares Support Vector Machines, and Extreme Learning Machine, first ed., Elsevier Inc., 2017, <https://doi.org/10.1016/B978-0-12-811318-9.00018-1>.
- [59] J. Kennedy, R. Eberhart, Particle swarm optimization, in: Proc. ICNN'95-International Conf. Neural Networks, IEEE, 1995, pp. 1942–1948.
- [60] Deep Kusum, Bansal Jagdish Chand, Mean particle swarm optimisation for function optimisation, *Comput. Intell.* 1 (2009) 72–92.
- [61] X. Zhou, D.J. Armaghani, J. Ye, M. Khari, M.R. Motahari, Hybridization of parametric and non-parametric techniques to predict air over-pressure induced by quarry blasting, *Nat. Resour. Res.* (2020) <https://doi.org/10.1007/s11053-020-09714-3>.
- [62] X.N. Bui, H. Nguyen, H.A. Le, H.B. Bui, N.H. Do, Prediction of blast-induced air over-pressure in open-pit mine: Assessment of different artificial intelligence techniques, *Nat. Resour. Res.* 29 (2020) 571–591, <https://doi.org/10.1007/s11053-019-09461-0>.
- [63] S. Liou, C. Wang, Integrative discovery of multifaceted sequence patterns by frame-relayed search and hybrid PSO-ANN, 15, 2009, pp. 742–764.
- [64] A. Ratnaweera, S.K. Halgamuge, H.C. Watson, Self-organizing hierarchical particle swarm optimizer with time-varying acceleration coefficients, *IEEE Trans. Evol. Comput.* 8 (2004) 240–255, <https://doi.org/10.1109/TEVC.2004.826071>.
- [65] A.A. Heidari, S. Mirjalili, H. Faris, I. Aljarah, M. Mafarja, H. Chen, Harris hawks optimization: Algorithm and applications, *Future Gener. Comput. Syst.* 97 (2019) 849–872, <https://doi.org/10.1016/j.future.2019.02.028>.
- [66] S. Mirjalili, S.M. Mirjalili, A. Lewis, Grey Wolf optimizer, *Adv. Eng. Softw.* 69 (2014) 46–61, <https://doi.org/10.1016/j.advengsoft.2013.12.007>.
- [67] S. Li, H. Chen, M. Wang, A.A. Heidari, S. Mirjalili, Slime mould algorithm: A new method for stochastic optimization, *Future Gener. Comput. Syst.* 111 (2020) 300–323, <https://doi.org/10.1016/j.future.2020.03.055>.
- [68] A.H. Gandomi, A.H. Alavi, A new multi-gene genetic programming approach to non-linear system modeling. part ii: Geotechnical and earthquake engineering problems, *Neural Comput. Appl.* 21 (2012) 189–201, <https://doi.org/10.1007/s00521-011-0735-y>.
- [69] A.H. Gandomi, A.H. Alavi, A new multi-gene genetic programming approach to nonlinear system modeling. Part I: Materials and structural engineering problems, *Neural Comput. Appl.* 21 (2012) 171–187, <https://doi.org/10.1007/s00521-011-0734-z>.
- [70] M. Dorn, A.L.S. Braga, C.H. Llanos, L.S. Coelho, A GMDH polynomial neural network-based method to predict approximate three-dimensional structures of polypeptides, *Expert Syst. Appl.* 39 (2012) 12268–12279.
- [71] A.G. Ivakhnenko, Polynomial theory of complex systems, *IEEE Trans. Syst. Man. Cybern.* (1971) 364–378.
- [72] T.N. Nguyen, S. Lee, H. Nguyen-Xuan, J. Lee, A novel analysis-prediction approach for geometrically nonlinear problems using group method of data handling, *Comput. Methods Appl. Mech. Engrg.* 354 (2019) 506–526, <https://doi.org/10.1016/j.cma.2019.05.052>.
- [73] I. Ebtehaj, H. Bonakdari, A.H. Zaji, H. Azimi, F. Khoshbin, GMDH-type neural network approach for modeling the discharge coefficient of rectangular sharp-crested side weirs, *Eng. Sci. Technol. Int. J.* 18 (2015) 746–757, <https://doi.org/10.1016/j.jestch.2015.04.012>.
- [74] G. Raghuram, A. Verma, *ScienceDirect Dedicated Freight Corridor: Current Challenges*, 2019.
- [75] P.G. Asteris, V.G. Mokos, Concrete compressive strength using artificial neural networks, *Neural Comput. Appl.* 32 (2020) 11807–11826, <https://doi.org/10.1007/s00521-019-04663-2>.
- [76] N. Kardani, A. Bardhan, D. Kim, P. Samui, A. Zhou, Modelling the energy performance of residential buildings using advanced computational frameworks based on RVM, GMDH, ANFIS-BBO and, *J. Build. Eng.* 35 (2021) 102105, <https://doi.org/10.1016/j.jobe.2020.102105>.
- [77] M. Kumar, A. Bardhan, P. Samui, J.W. Hu, M.R. Kaloop, Reliability analysis of pile foundation using soft computing techniques: A comparative study, *Processes* 9 (2021) <https://doi.org/10.3390/pr9030486>.
- [78] N. Kardani, A. Bardhan, P. Samui, M. Nazem, A. Zhou, D.J. Armaghani, A novel technique based on the improved firefly algorithm coupled with extreme learning machine (ELM-IFF) for predicting the thermal conductivity of soil, *Eng. Comput.* (2021) <https://doi.org/10.1007/s00366-021-01329-3>.
- [79] M.N. Kardani, A. Baghban, M.E. Hamzehie, M. Baghban, Phase behavior modeling of asphaltene precipitation utilizing RBF-ANN approach, *Pet. Sci. Technol.* 37 (2019) 1861–1867.
- [80] N. Kardani, A. Zhou, M. Nazem, S.L. Shen, Improved prediction of slope stability using a hybrid stacking ensemble method based on finite element analysis and field data, *J. Rock Mech. Geotech. Eng.* 13 (2021) 188–201, <https://doi.org/10.1016/j.jrmge.2020.05.011>.
- [81] N. Kardani, A. Zhou, M. Nazem, X. Lin, Modelling of municipal solid waste gasification using an optimised ensemble soft computing model, *Fuel* 289 (2021) 119903.
- [82] S. GHANI, S. KUMARI, A. BARDHAN, A novel liquefaction study for fine-grained soil using PCA-based hybrid soft computing models, *Sādhāraṇā* 46 (2021) 113, <https://doi.org/10.1007/s12046-021-01640-1>, In this issue.
- [83] R. Kumar, M.P. Singh, B. Roy, A.H. Shahid, A Comparative Assessment of Metaheuristic Optimized Extreme Learning Machine and Deep Neural Network in Multi-Step-Ahead Long-Term Rainfall Prediction for All-Indian Regions, Springer Netherlands, 2021, <https://doi.org/10.1007/s11269-021-02822-6>.
- [84] B. Roy, M.P. Singh, A. Singh, A novel approach for rainfall-runoff modelling using a biogeography-based optimization technique, *Int. J. River Basin Manag.* (2019) 1–14, <https://doi.org/10.1080/15715124.2019.1628035>.
- [85] J. Duan, P.G. Asteris, H. Nguyen, X.N. Bui, H. Moayedi, A novel artificial intelligence technique to predict compressive strength of recycled aggregate concrete using ICA-XGBoost model, *Eng. Comput.* (2020) <https://doi.org/10.1007/s00366-020-01003-0>.
- [86] K.E. Taylor, Summarizing multiple aspects of model performance in a single diagram, *J. Geophys. Res. Atmos.* 106 (2001) 7183–7192, <https://doi.org/10.1029/2000JD900719>.
- [87] A. Gholami, H. Bonakdari, P. Samui, M. Mohammadian, B. Gharabaghi, Predicting stable alluvial channel profiles using emotional artificial neural networks, *Appl. Soft Comput.* 78 (2019) 420–437.
- [88] P.G. Asteris, A.D. Skentou, A. Bardhan, P. Samui, Cement and concrete research predicting concrete compressive strength using hybrid ensembling of surrogate machine learning models, *Cem. Concr. Res.* 145 (2021) 106449, <https://doi.org/10.1016/j.cemconres.2021.106449>.